CHAPTER 11

Bulk Models of Solidification

Herbert E. HUPPERT

Institute of Theoretical Geophysics, Department of Applied Mathematics and Theoretical Physics, Silver Street, Cambridge, UK CB3 9EW

Contents

HANDBOOK OF CRYSTAL GROWTH, VOL. 1
edited by D.T.J. Hurle

1. Introduction

Many of the studies discussed in this Handbook consider the physics and chemistry of growth of single crystals. In many different natural and industrial situations, however, a melt of large volume cools and gradually solidifies simultaneously at many different sites. In this way, a very large array of crystals are grown. For example, the liquid outer core of the earth is currently solidifying at a rate of the order of 2×10^6 kg s^{-1} of almost pure iron on the surface of the solid inner core. Rather than follow the interactive growth of each particular crystal, it is often advantageous, if not essential, to consider bulk models which govern the overall properties of the resultant solid. An analogy can be drawn here with the many-bodied problem of a large number of moving gas molecules considered by physicists and the continuum mechanics approach taken by fluid dynamicists.

This chapter reviews some of the approaches that have been developed to investigate the growth of solid on scales considerably larger than the microscale. Some of the concepts of microscale solidification, considered elsewhere in this Handbook, will enter into the discussion in order to support the main aim of this chapter which is to describe the overall rate of growth of solid and the macroscopic form taken by the solid product. Fluid-mechanical effects can have a dominant role in solidification problems and, so, fundamental concepts of fluid mechanics will permeate the discussion. One of the ways that fluid-mechanical effects are important is a result of the fact that when a liquid of two or more components solidifies, the composition of the solid product generally differs from that of the original liquid. For example, salty water in the polar oceans freezes to form almost pure ice, while semiconductor melts containing comparable quantities of tin and silicon could be partially solidified to form almost pure silicon. The difference in composition between liquid and solid implies that the composition of the liquid in the neighbourhood of the solidification front can be different from that further away. This difference in composition is generally associated with a difference in density, which can drive fluid motions, transport both heat and mass convectively and alter the rate and maybe even the mode of the solidification processes.

This chapter considers sequentially a series of situations, each of which includes and illustrates new effects. A number of these have been discussed, from a slightly different point of view, by Huppert [1] in a publication which includes numerous colour photographs. In section 2 the uniform cooling from below, of a liquid which is compositionally identical to its solidified product, is discussed. This one-dimensional problem is one of the simplest examples of a classical Stefan problem and has no fluid-mechanical ingredient. The stability of this system is briefly reviewed in the next section. As we shall describe there, many solidification problems display a range of instabilities, which result in thermal and compositional convection as well as morphological instability of the resulting, solidifying interface which one might have supposed to be locally planar. This surface instability often results in the formation of a *mushy layer*, which is a layer of solid dendrites bathed in interstitial liquid. Much recent research has been devoted to developing equations that describe the macroscopic evolution of such mushy layers, which fit comfortably between the purely solid and completely fluid ends of continuum mechanics.

Section 4 analyses the effects of an unstable thermal field and the convection this induces when the pure fluid considered in section 2 is cooled from above. These fundamental situations act as part of the foundation for the main body of the chapter, which focuses on effects due to compositional differences when a binary alloy is solidified in various geometries. We indicate that the simple, but paradigm, situations of cooling an initially homogeneous, two-component melt at a single horizontal boundary can be divided into a 2×3 array of six different regimes, dependent upon whether the cooling takes place at an upper or lower boundary to the melt, and whether the density of the fluid released on solidification is the same as, less than or greater than that of the melt.

We first consider the cooling and crystallizing from below, of a liquid that releases fluid of greater density upon solidification. In this situation the moving interface between fluid and solid is generally unstable, which leads to the formation of a mushy layer. We then develop the concepts and governing equations which describe mushy layers and demonstrate that predictions can be obtained which agree well with data from laboratory experiments. The theoretical concepts are then extended to a study of the solidification that results from cooling from above a liquid which releases less dense fluid. Assuming first that solidification occurs at thermodynamic equilibrium, so that the temperature at the solidifying interface is equal to the specified equilibrium solidification temperature, and that the cooling temperature exceeds the eutectic temperature, we explain how to determine the rate of growth of the mushy layer that forms on the roof. The agreement between the theoretical predictions and the laboratory data is good, but not perfect. The agreement can be improved by the incorporation of nonequilibrium effects into the model by specifying a relationship between the rate of growth of the mushy layer and the nonequilibrium undercooling at the interface between mush and liquid. Effects due to lowering the cooling temperature below the eutectic temperature are then discussed. We describe how this can lead to compositional stratification in the solid. In addition, we explain how cooling at the top of a container can lead to solidification at the base – a result relevant to the cooling of a large magma chamber, or storage chamber of liquid rock, from above. Global two-dimensional effects, which result from cooling at either a vertical or a sloping wall, are discussed in sections 6 and 7.

2. *Static solidification of a pure substance: the classical Stefan problem*

We shall commence the development with a description of the simplest situation in which a pure melt undergoes a phase change and is transformed into a solid. The resulting mathematical model is the simplest example of a "Stefan problem", a name which commemorates the early work of Stefan, published in 1889 [2]. Consider the semi-infinite region in $z > 0$ to consist of material which is initially totally liquid and is at uniform temperature T_∞. Assume that at $t = 0$ the temperature at the base of the fluid (at $z = 0$) is suddenly lowered to T_B and maintained at that value, which is less than the solidification temperature of the melt, T_M. The problem is to determine the position of the unknown solidifying interface $s(t)$ and the resulting temperature

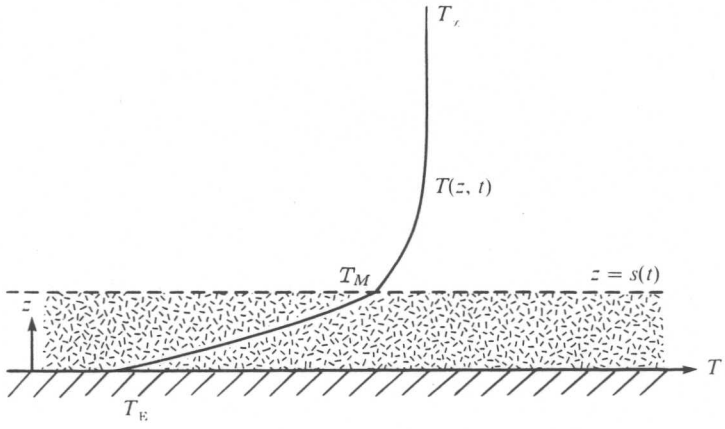

Fig. 1. Sketch of the temperature profile, the resulting one-dimensional solid layer and the notation for a semi-infinite, one-component liquid cooled from below.

distributions $T(z, t)$ in both the liquid and the solid phases in this solely one-dimensional problem. A sketch of the geometry and temperature field is given in fig. 1.

The analysis commences with the assumption that there is no motion in the melt and that compositional effects play no role in the resultant solidification. This requires the constituents of the melt and the solid to be identical. Generally, this means a one-component, or pure, melt, such as water or liquid gold, for example. However, in addition, binary melts of a eutectic composition also produce solids that have the same composition as the original liquid. Throughout the discussion, we shall neglect any difference in density between solid and liquid, which can often be a small effect. A brief discussion of such effects is presented by Worster [3].

Mathematically, the problem requires the solution of the heat conduction equations as outlined in chapter 10. For our purposes these are expressed as

$$\frac{\partial T}{\partial t} = \kappa_s \frac{\partial^2 T}{\partial z^2} \quad (0 < z \leqslant s(t)), \tag{2.1a}$$

$$\frac{\partial T}{\partial t} = \kappa_\ell \frac{\partial^2 T}{\partial z^2} \quad (s(t) \leqslant z), \tag{2.1b}$$

where κ is the thermal diffusivity, with subscripts s and ℓ denoting values in the solid and liquid, respectively. The regions occupied by the two phases are linked by the conservation of heat flux at the interface, which can be written as

$$\mathscr{L} \frac{ds}{dt} = K_s \frac{dT}{dz}\bigg|_{s-} - K_\ell \frac{dT}{dz}\bigg|_{s+}, \tag{2.2}$$

where $\mathscr{L}$ is the latent heat per unit volume of solid and K is the thermal conductivity. Finally, there are the boundary conditions on the temperatures

$$T = T_B \quad (z = 0), \quad T = T_M \quad (z = s), \qquad T \to T_\infty \quad (z \to \infty \text{ or } t \to 0). \tag{23a, b, c}$$

Because there is no externally imposed length scale in the problem, the solution must

be representable in terms of the similarity variable

$$\eta = \tfrac{1}{2} z/(\kappa_s t)^{1/2} \tag{2.4}$$

and the solution must be of the form

$$s(t) = 2\lambda_2(\kappa_s t)^{1/2}, \tag{2.5}$$

with λ_2 satisfying an eigenvalue relationship of the form

$$F\left(\lambda_2; S, \frac{T_\infty - T_M}{T_M - T_B}, \frac{K_s}{K_\ell}, \frac{\kappa_s}{\kappa_\ell}\right) = 0, \tag{2.6}$$

where the Stefan number

$$S = \frac{\mathscr{L}}{c_s(T_M - T_B)} \tag{2.7}$$

and c_s is the specific heat per unit volume of the solid. The Stefan number represents the ratio of two quantities: the latent heat needed to transform the melt into solid and the heat needed to cool the solid from its solidification temperature to the temperature at the boundary. The parameter $\mathscr{H} = (T_\infty - T_M)/(T_M - T_B)$ is sometimes called the nondimensional superheat because it is a (nondimensional) representation of the amount by which the melt is heated above its solidification temperature.

Explicit relationships for the temperature field and the function F that appears in eq. (2.6) are given in Charslaw and Jaeger [4, section 11.2]. One of the simplest cases to consider is $T_\infty = T_s$ (which corresponds to the melt being initially at the solidification temperature and the superheat being zero), $K_s = K_\ell$ and $\kappa_s = \kappa_\ell$ (the thermal properties of melt and solid are identical). In this case

$$T(z, t) = T_B + (T_M - T_B)\,\mathrm{erf}\,\eta/\mathrm{erf}\,\lambda \tag{2.8}$$

and

$$F(\lambda, S) = \pi^{1/2}\lambda e^{\lambda^2}\,\mathrm{erf}\,\lambda - S^{-1} \tag{2.9a}$$

$$\equiv f(\lambda) - S^{-1}, \tag{2.9b}$$

where $\mathrm{erf}\,\eta$ is the error function [5]. Figure 2 presents a graph of the monotonically increasing function $f(\lambda)$ as a function of λ, from which it can be seen immediately that there exists a unique solution for all (positive) values of S.

The solution (2.6) appears to have been first presented by Lamé and Clapeyron in 1831 [6]. It was then discussed in a famous series of (unpublished) lectures given by Neumann in Königsberg in the early 1860s and reappeared in Stefan's article [2], which gave rise to the general name of Stefan problem being used to describe in a rather loose way a huge variety of moving-boundary problems, which often, but not always, involve melting and solidification. Very few exact analytical solutions exist and, generally, either approximate or numerical methods are required to determine the solution to a particular problem. The book by Hill [7] presents an admirable introduction to the subject and further developments can be found in Crank [8].

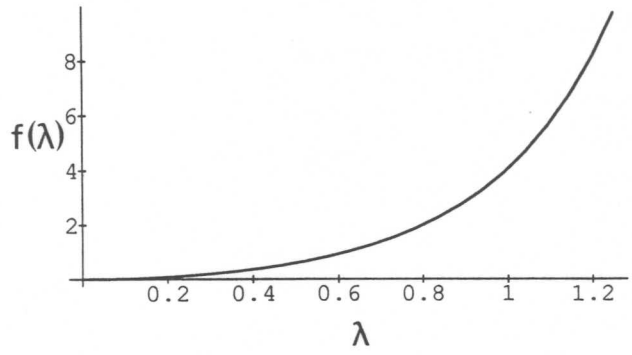

Fig. 2. Graph of $f(\lambda) = \pi^{1/2}\lambda e^{\lambda^2}\,\mathrm{erf}\,\lambda$ as a function of λ. The eigenvalue relationship $f(\lambda) = S^{-1}$ for the paradigm Stefan problem has a unique solution for all $S > 0$.

A common, and often useful, simplification employed is to assume that the Stefan number S is very large. Large values of S, which can be considered to reflect large values of the latent heat $\mathscr{L}$ for fixed values of the undercooling, $T_M - T_B$, correspond to small values of ds/dt, and, hence, slow solidification, as indicated by eq. (2.2). In nondimensional terms, this means that solidification takes place over a timescale that is large compared to the time taken for the temperature field to adjust by thermal diffusion. Thus, the temperature field is quasi-stationary and a suitable approximate solution of eqs. (2.1a) and (2.3a, b) in the particularly simple paradigm problem considered above is

$$T(z, t) = T_B + (T_s - T_B)z/s(t). \tag{2.10}$$

Insertion of eq. (2.10) into eq. (2.2) leads to the solution

$$s(t) = (2\bar{\kappa}_s t)/S)^{1/2}, \quad [\lambda = (2/S)]^{1/2}, \tag{2.11a, b}$$

which is identical to the result obtained on letting $S \to \infty$ in eq. (2.9a). The concept that for large S the temperature field is linear in z [cf. eq. (2.10)] can be very useful and a chapter of Hill [7] is devoted to explaining how to exploit techniques based on this approximation.

Alternatively, in some Stefan problems small values of S can raise great difficulties. This is because eq. (2.2), when associated with a small value of $\mathscr{L}$, suggests the occurrence of a singular perturbation problem in which $s(t)$ varies rapidly. An example is given by the initial-value problem that arises when hot fluid begins to flow turbulently over a solid basement that can melt. Examples of such behaviour include the pouring of hot water over cold ice or hot chocolate over cold icecream. A power-series representation of the resultant position of the interface can be written [9] as

$$\eta(\tau) = \sum_{n=1}^{\infty} \eta_{n-1}\tau^{n/2}, \tag{2.12}$$

where $\eta(\tau)$ is the nondimensional position of the interface in terms of a nondimensional time τ. The expansion coefficients η_n as a function of the Stefan number are graphed in fig. 3. For S greater than unity the representation converges rapidly, while

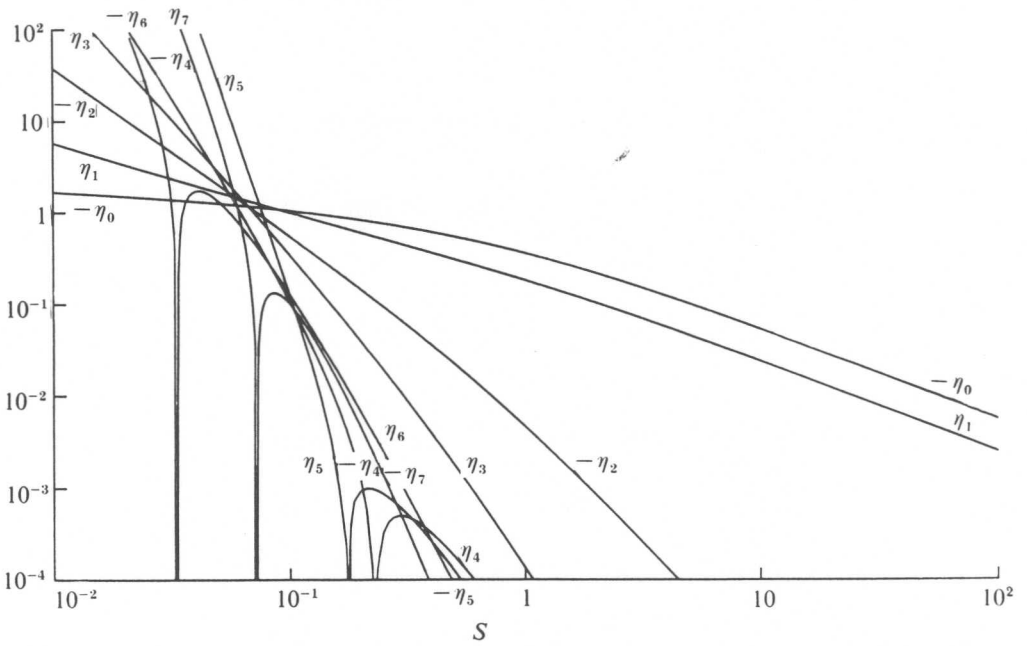

Fig. 3. Curves of the expansion coefficients η_n for $n = 0$–7 as functions of the Stefan number S used in a description of the interaction between a hot, turbulently flowing liquid and a cold solid substrate.

for small S the coefficients oscillate rapidly, reflecting the rapid change in motion of the interface. There are some problems, however, for which ds/dt does not become large as $S \to 0$. Instead, the right-hand side of eq. (2.2) is approximately zero, the interpretation of which is that the heat fluxes on either side of the interface approximately balance without any significant contribution from the latent heat release. The position of the interface can then be determined by solving a pure conduction problem and inserting the interface at the position of the isotherm $T = T_M$. No general criteria seems yet to have been obtained to decide a priori which of these two situations will occur for small S.

3. Stability

All the analysis has so far been strictly one-dimensional, reflecting the absence of variations of the cooling and the container geometry in the other two dimensions. However, it is conceivable that the resulting solutions are unstable, i.e., there are additional solutions which do have variations in the horizontal plane. Dynamical systems are awash with such instabilities. Rather than describe a rigorous mathematical analysis of the appropriate problems, it is more useful for our purposes to conduct a physical appraisal of the instability and refer the reader to chapter 12 and references therein for analytical details. Consider a flat solidifying surface to be perturbed and to take up the two-dimensional shape sketched in fig. 4. The perturbed curves of constant temperature are also sketched. Near the furthest point A, the isotherms are relatively

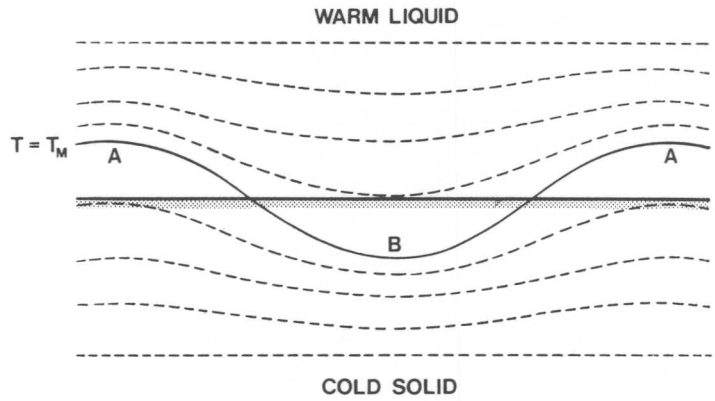

Fig. 4. A sketch of the one-dimensional planar interface between solid and liquid (shown stippled), the sinusoidal perturbation to it (solid curve) along which the temperature is constant, and the resulting isotherms (dashed curves), when a relatively warm liquid is solidified. Thermal fluxes are enhanced in regions where the isotherms are compressed and reduced in regions where they are expanded. The solid is, thereby, preferentially melted back near A and preferentially deposited near B, resulting in a decrease of the perturbation.

compressed in the melt and sparse in the solid. Thus, the additional heat flux into the melt is positive and that from the solid is negative. The perturbation, hence, tends to melt back solid at A. Using a similar argument, it can be shown easily that the perturbation tends to solidify material preferentially at B. The overall result is that the one-dimensional solution is recovered, i.e., it is stable. This physical argument of stability suggests that it is not necessary to present a rigorous mathematical analysis at this point.

The result is, however, seemingly at odds with our experience of many natural solidification processes wherein the solidifying surface is irregular, such as in snow flakes and solidifying moulds. The explanation is seen immediately with a simple alteration to the above physical description: the solidification surface is now assumed to penetrate an undercooled liquid, in which the temperature is less than the solidification temperature, Such a situation is a frequent occurrence and gives rise to the physical sketch of fig. 5. Consider first the simple case, sketched in fig. 5a, in which the solid is at uniform temperature T_M, the solidification temperature. In this case the perturbation of the isotherms leads to an increased heat transfer to the melt at A and a decreased transfer at B, thus accentuating the departure from the flat interface. This destabilizing effect is countered by the Gibbs–Thomson process, described in chapter 12, which causes the temperature at A to decrease because of the curvature, while the temperature at B increases. Heat, thus, flows away from B, which promotes solidification and counteracts the dominant destabilizing process.

The destabilization, which is due to thermal diffusion, is most effective on the length scale of thermal diffusion, which is $l_D = \kappa/V$, where V is the velocity of propagation of the solidifying surface. The stabilization due to the Gibbs–Thomson effect operates most strongly on the length scale $l_{GT} = \Gamma/\mathscr{S}$, where Γ is the surface tension divided by the entropy of fusion and $\mathscr{S}$ is the Stefan number $\mathscr{L}/c(T_M - T_\infty)$. A formal linear

stability analysis (chapter 12 and [10]) to determine the perturbation quantities of the form $e^{i\boldsymbol{k}_H \cdot \boldsymbol{x} + \sigma t}$, where $\boldsymbol{k}_H$ is the horizontal wavenumber, indicates that there is a relationship between σ and the magnitude of the wavenumber $k = |\boldsymbol{k}_H|$ of the form

$$\sigma = Vk(1 - 2l_D l_{GT} k^2), \tag{3.1}$$

as sketched in fig. 5b. The shape of the curve reflects the fact that the basic solution must be recovered at $k = 0$ (and, hence, $\sigma = 0$ there) and that stabilizing Gibbs–Thomson effects dominate for small wavelengths ($k \to \infty$). The maximum unstable growth rate $\sigma_{max} = \frac{2}{3} \times 6^{-1/2} V(l_D l_{GT})^{-1/2}$ is attained at a wavelength $\lambda = 2 \times 6^{1/2} \pi (l_D l_{GT})^{1/2}$ which is proportional to the geometric mean of the length scales of diffusion and surface tension.

A number of other physical systems have exactly the same stability curve as eq. (3.1). These include the famous Saffman–Taylor instability which occurs when a fluid forces out a more viscous fluid in a Hele–Shaw cell [11] and diffusion-limited aggregation [12], in which random walkers on a square grid remain at a particular site if a neighbouring site is already occupied. Both these problems, and the solidification problem, are beautifully drawn together in a review by Couder [13].

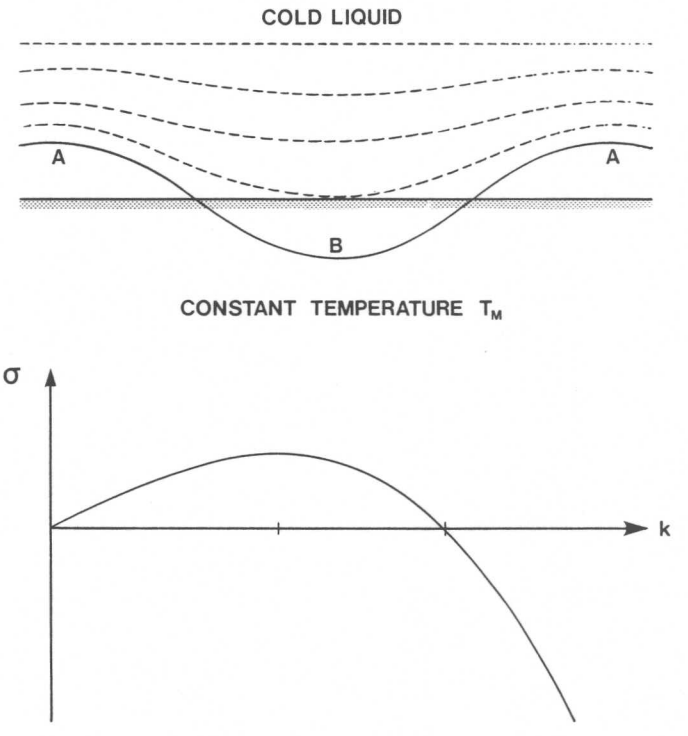

Fig. 5. (a) With the notation of fig. 4, a solid is advancing into a undercooled liquid. The altered thermal transfers are now such that solid is preferentially deposited near A while near B solid is deposited less rapidly. Surface tension effects, dominant over small length scales, decrease the temperature at A over that at B, leading to a heat flow from B to A which stabilizes small-wavelength perturbations. (b) The dispersion relationship $\sigma = Vk(1 - 2l_D l_{GT} k^2)$ resulting from an analysis of the stability mechanism described in the description of (a).

4. *The solidification of a pure melt from above*

Inverting the geometry from that considered in section 2, as sketched in fig. 6, leads to quite a different situation; in particular, strong fluid-mechanical effects are incorporated. These arise because the resulting temperature in the liquid increases with depth and, thus, a convective instability in the liquid is possible. A combined experimental and theoretical investigation of the conditions for which instability is initiated and the form of convection in the liquid has been carried out by Davis et al. [14] and Dietsche and Müller [15]. They held fixed the temperatures T_A and T_B at the lower and upper boundaries, as depicted in fig. 6a, and determined from the solution of a steady-state problem the critical value of the Rayleigh number

$$Ra = \alpha g(T_A - T_s)(H - s)^3/\kappa_\ell \nu \tag{4.1}$$

for the onset of convection as a function of the ratio $\mathscr{A}$ of the depths of solid and liquid in static equilibrium, with

$$\mathscr{A} = \frac{s}{H - s} = \left(\frac{K_s}{K_\ell}\right)\left(\frac{T_s - T_B}{T_A - T_s}\right), \tag{4.2a, b}$$

where α is the coefficient of expansion, g the acceleration due to gravity and H the total depth of the system. They then employed weakly nonlinear perturbation theory to predict the form of the convective motions – rolls, hexagons or mixed polygonal rolls – for Rayleigh numbers just above the critical point. These theoretical predictions were in good qualitative agreement with their experiments using cyclohexane, which showed picturesque defomations at the interface between solid and melt due to convection coupled to the melting and freezing.

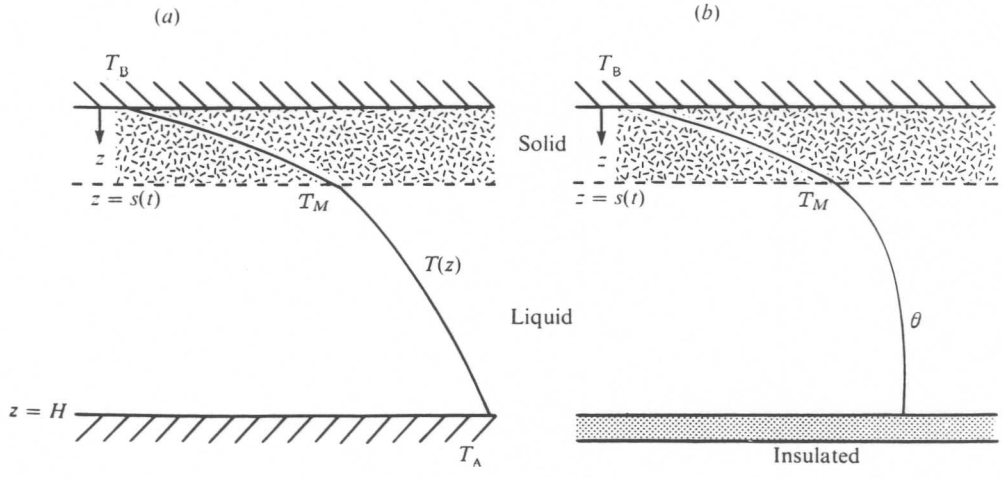

Fig. 6. Sketch of the temperature profile and the notation for an initially homogeneous, one-component liquid of initial depth H cooled from above. Note that in (a) the lower boundary is at a fixed temperature while in (b) the lower boundary is insulated.

Because of their analytical tractability, numerous theoretical studies of directional solidification have been undertaken using the techniques of weakly nonlinear perturbation theory (see, e.g., the work of Coriell et al. [16]). There has been some agreement between the theoretical results of these studies and experimental observations, but, generally, in natural, industrial and even in most laboratory experimental situations, the conditions are well away from those for which weakly nonlinear theory is applicable. When, e.g., in the geometry considered by Davis et al. [14], the Rayleigh number is very much larger than the critical value and sufficiently high for the convection in the liquid to be turbulent, a different parameterization to the one they considered is appropriate. Turner et al. [17] and Huppert and Worster [18] examined the situation depicted in fig. 6b, where the lower boundary is insulated, rather than being maintained at a fixed temperature. This allows the temperature to evolve with time and leads eventually to total solidification. The relevant conduction equation in $0 < z \leqslant s(t)$ is again given by eq. (2.1a). In the liquid the heat transfer can be described by the well-known four-thirds law [19], so that

$$-c_\ell(H-s)\frac{\mathrm{d}\theta}{\mathrm{d}t} = F_T = \gamma K_\ell \left(\frac{\alpha g}{\kappa_\ell \nu}\right)^{1/3} (\theta - T_s)^{4/3}, \tag{4.3a, b}$$

where θ is the mean temperature of the liquid, F_T is the thermal flux at the interface and γ is an empirical constant with a value of approximately 0.14. The interfacial condition [cf. (2.2)] is

$$K_s \left.\frac{\mathrm{d}T}{\mathrm{d}z}\right|_{s-} = F_T + [c_\ell(\theta - T_s) + \mathscr{L}]\frac{\mathrm{d}s}{\mathrm{d}t}. \tag{4.4}$$

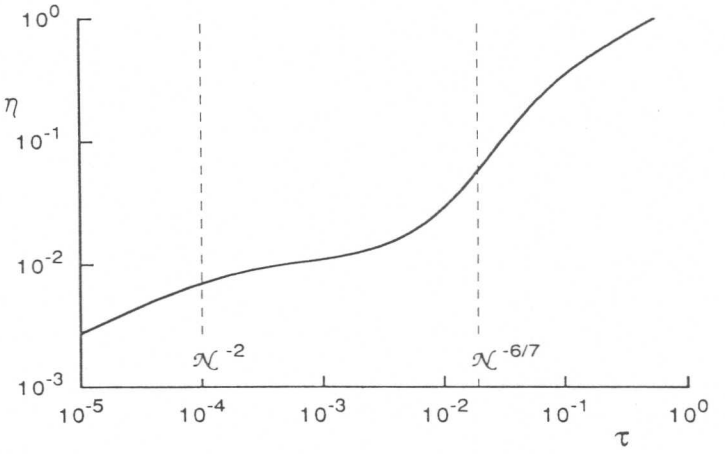

Fig. 7. Typical results of numerical calculations of the resulting nondimensional thickness $\eta = s/H$ as a function of the nondimensional time $\tau = \kappa_\ell t/H^2$ due to solidification of a layer of liquid cooled from above. In the results presented, the dimensionless parameter $\mathcal{N} = 100$. The depth of the solid layer as a function of time is shown on logarithmic axes to illustrate the different stages of evolution. The vertical dashed lines indicate the approximate transition times as determined by asymptotic analysis between three distinct regimes.

This equation represents a balance of the conductive transfer through the solid with the convective transfer in the liquid plus the heat released by decreasing the temperature of the melt to the solidification temperature and then solidifying it. Each of these terms is always positive and, so, in particular, the term on the left-hand side always contributes in an essential way to the heat balance. Either of the other two terms may also dominate the heat balance and this leads to three different regimes. Within each regime, conduction balances either convection, latent heat release, or both, as discussed at length by Turner et al. [17]. They present both asymptotic and numerical solutions to the equations as well as data from a variety of experiments which, as far as they go, support the theoretical predictions. It would be interesting to carry out further experiments in parameter ranges different from those treated experimentally by Turner et al. [17] yet falling within the range of their theory.

Huppert and Worster [18] took the investigation one stage further by considering the analysis for large values of the initial Rayleigh number Ra_0. They determined analytic solutions for each of the three ranges. Their results are summarized in fig. 7, which presents the nondimensional solid thickness $\eta = s/H$ as a function of the nondimensional time $\tau = \kappa_l t/H^2$. Also shown are the approximate transition times between the three regimes discussed in the previous paragraph, as determined by the asymptotic analysis, of $\mathcal{N}^{-2}$ and $\mathcal{N}^{-6/7}$, where $\mathcal{N} = \gamma Ra_0^{1/3}$.

5. *Solidification of a binary alloy*

5.1. *General framework*

When there are two (or more) components in the melt, a whole range of new effects can take place. Some of these will be described in the next section. Multicomponent melts occur frequently in both industrial and natural situations. For example, bronze and brass are mixtures of copper and lead, tin or zinc. In a geological context, molten rock (magma within the earth and lava once it has been extruded from it) is a silicate mixture with many components [20, 21].

The study of any solidification problem of a two- (or more-) component melt must commence with a study of the phase diagram. A typical phase diagram for a two-component melt is presented in fig. 8a and a general description of phase equilibria is given in chapter 2. Figure 8b indicates the simplification that is often present for aqueous solutions, for which the solidi are vertical. Incorporation of this fact can simplify the theoretical analysis considerably. Given, in addition, that laboratory experiments with aqueous solutions are very much easier to handle than either metallic alloys or binary organic liquids, the building and confirmation of models using aqueous solutions makes for a very satisfactory scientific procedure.

When there are any fluid-mechanical processes operative in the solidification, the (changing) density of the melt can play a fundamental role. For this reason, the lines of constant density have been included in the phase diagrams. Typically, as shown in the figure, density in the melt is a very much stronger function of composition than of temperature, as measured by the fact that the slopes of lines of constant density are

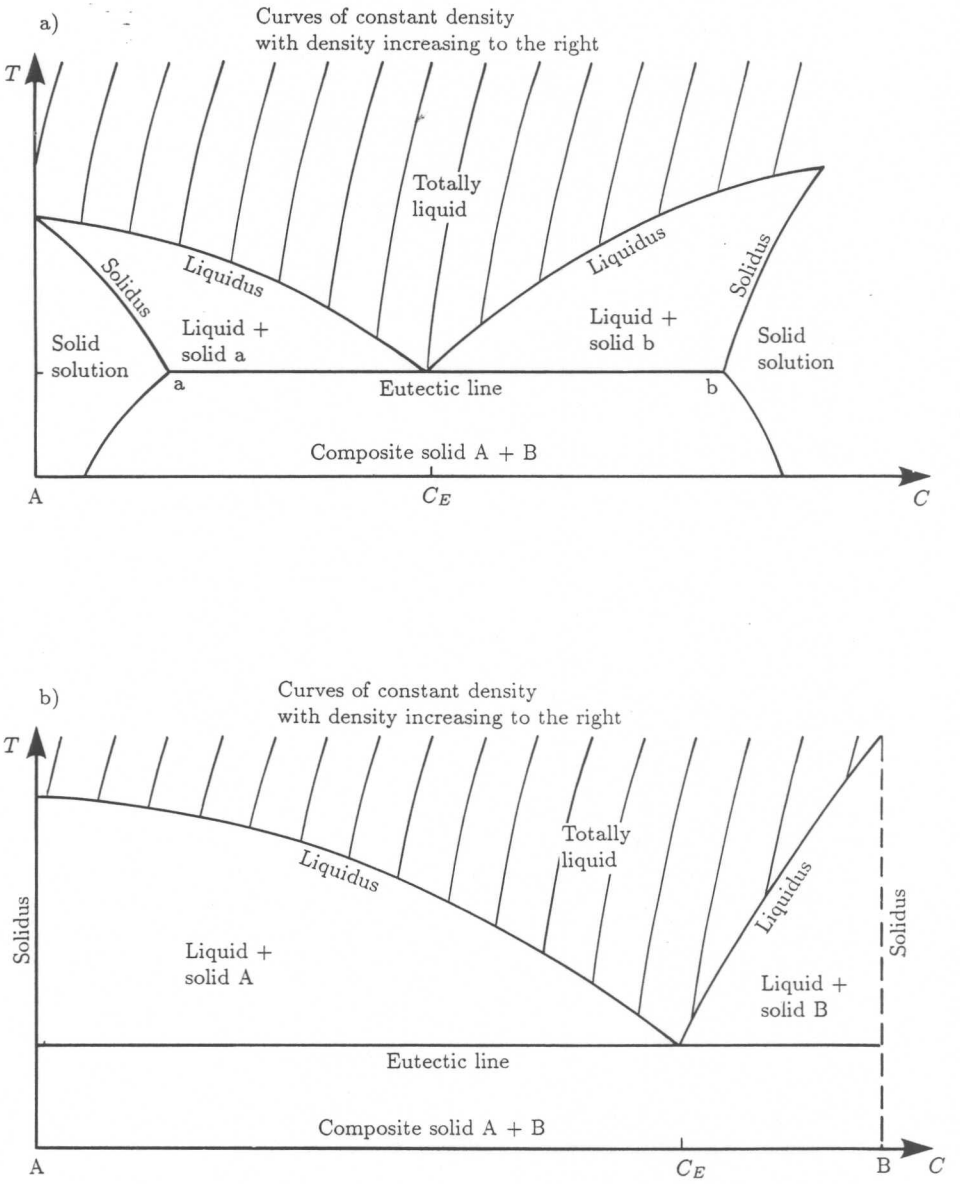

Fig. 8. Typical phase diagrams for binary alloys made up of components A and B, which indicate the phases as functions of the temperature T and the concentration of the component B, which is denoted by C. In (b), which is a special case of (a), the solidi are vertical, reflecting the fact that the concentration in the solid is constant and independent of the temperature at which it was formed. Almost all aqueous solutions have phase diagrams of the type (b).

much closer to being vertical (indicating little change with temperature) than are the slopes of either of the liquidi. This effect can play an important dynamical role as follows. Consider a melt whose composition is less than the eutectic composition (a subeutectic melt) which is cooled and solidifies, with component A being preferentially taken into the solid. As the temperature decreases, the liquid released at the site of solidification is of a greater density than that far away. Depending upon the geometri-

Table 1

A summary of the six different regimes that occur when a two-component melt is cooled at a horizontal boundary. The three different compositional conditions are tabulated in the first column and the effect this has on the fluid released by the resultant solidification is tabulated in the last column. The two different thermal conditions are tabulated in the first row and the effect this has on the stability of the resulting thermal field in the melt is tabulated in the last row. The interior 3×2 array summarizes sequentially the major effect in each situation, as well as indicating in which section of the text it is treated.

Compositional constraint	Cooling from		Effect of composition
	Below	Above	
1. $C < C_E$ or $C = C_A$	3. Stagnant melt and mushy layer (section 5.2)	6. Convection in melt driven by both thermal and compositional effects	Relatively heavy fluid released
2. $C = C_E$	1. Classical Stefan problem (section 2)	2. Thermally driven convection in liquid possible (section 3)	Fluid density depends only on temperature
3. $C > C_E$ or $C = C_B$	5. Compositional convection in melt (section 5.5)	4. Thermally driven convection in melt beneath a stagnant mushy layer (section 5.4)	Relatively light fluid released
	Resulting thermal profile in melt		
	Stable	Unstable	

cal configuration, to be discussed further below, this density difference can drive strong convective motions which can influence the rate and mode of solidification. Similarly, if the initial composition of the melt exceeds that of the eutectic (a supereutectic melt), the density of the released fluid decreases as the solidification proceeds. In general, compositional buoyancy greatly exceeds thermal buoyancy, even though the solidification may be driven by thermal transfers.

Motivated by such possible convective processes, Huppert and Worster [22] constructed a 3×2 array to classify the possible responses when an initially homogeneous two-component melt is cooled at a single horizontal boundary. The results are summarized in table 1, which indicates the relative density of the fluid released when the initial composition is (1) less than (2) equal to or (3) greater than the eutectic composition. The distribution of the resulting thermal field is also indicated in table 1 depending upon whether the liquid is cooled from a lower or an upper boundary. The array also shows the section in which each situation is discussed.

5.2. *Cooling from below a subeutectic binary alloy*

Some of the fundamental fluid-mechanical effects due to compositional differences between melt and solid can now be drawn out in an investigation of the solidification that results from cooling from below a binary alloy whose initial composition is less

than the eutectic composition. The fluid released by the solidification is then relatively dense and, thus, ponds above the solid. For simplicity consider the resultant solid to be of fixed composition (a vertical solidus) as will result, e.g., if ice is formed from the cooling of an aqueous solution. Assume also, at least initially, that the interface at $z = s(t)$ between solid and melt is flat (and horizontal) so that the problem is totally one-dimensional. No motion will occur in the melt and the transport of both heat and chemical components is entirely by molecular diffusion. This leads to profiles of both temperature and composition that are stably distributed, as sketched in fig. 9.

The equations governing the temperature profiles are exactly as in section 2. These are the heat conduction equation (2.1), the thermal conservation condition (2.2) and the thermal boundary conditions (2.3). The compositional profile relative to that in the solid, $C(z, t)$, is governed in the melt by

$$\frac{\partial C}{\partial t} = D\frac{\partial^2 C}{\partial z^2} \quad (s(t) \leqslant z), \tag{5.1}$$

where D is the coefficient of compositional diffusivity, while the (fixed) composition of the solid is expressed as $C = 0$. Conservation of solute requires that

$$s(t)C_\infty = \int_s^\infty (C - C_\infty)\,\mathrm{d}z, \tag{5.2}$$

from which, by differentiating eq. (5.2) and using eq. (5.1), it can be deduced that

$$C\frac{\mathrm{d}s}{\mathrm{d}t} + D\frac{\partial C}{\partial z} = 0 \quad (z = s(t) +). \tag{5.3}$$

The initial, or far-field, condition on the composition, to complement that on the temperature [eq. (2.3c)], is

$$C \to C_\infty \quad (z \to \infty \text{ or } t \to 0). \tag{5.4}$$

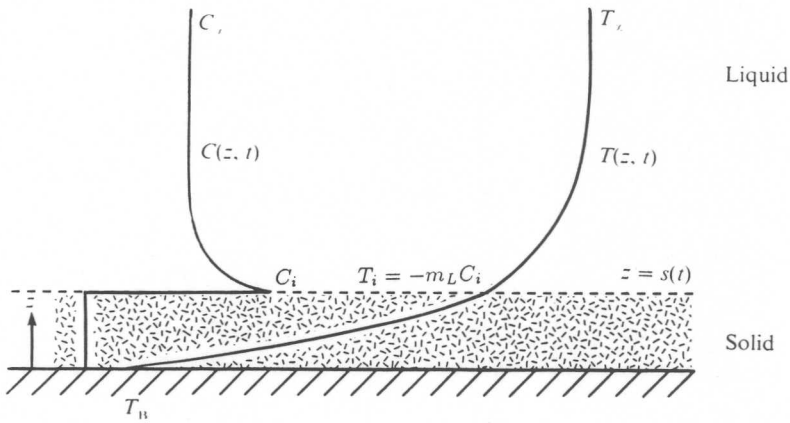

Fig. 9. Sketch of the stably distributed temperature and composition profiles for a semi-infinite binary melt cooled from below to form a stable one-dimensional interface between melt and solid on the release of melt whose density exceeds that of the original melt.

In a binary liquid that solidifies at thermodynamic equilibrium, the temperature of solidification T_M and the composition of the melt at the interface are connected by the liquidus relationship (see chapter 2). In many situations a linear relationship of the form

$$T = -m_L C, \tag{5.5}$$

where m_L is a positive constant, is an adequate approximation. Note that the form of eq. (5.5) assumes a temperature scale whose zero is equal to the melting temperature of the pure solvent (whose composition is zero).

Because there is no externally imposed length scale, the mathematical system (2.1)–(2.3), (5.1)–(5.4) and (5.5) applied at $z = s(t)$ admits a similarity solution of the form

$$s = 2\lambda_4 (Dt)^{1/2}, \tag{5.6}$$

with λ_4 satisfying an eigenvalue relationship of the form

$$F\left(\lambda_4; \tilde{S}, \frac{T_\infty - T_L}{T_L - T_B}, \frac{T_L}{T_B}, \frac{K_s}{K_\ell}, \frac{\kappa_s}{\kappa_\ell}, \frac{D}{\kappa_\ell}\right) = 0, \tag{5.7}$$

(see [22–24]), where the modified Stefan number

$$\tilde{S} = \frac{\mathscr{L}}{c_s(T_L - T_B)} \tag{5.8}$$

and $T_L = -m_L C_\infty$ is the liquidus temperature at the initial concentration. The resulting temperature and composition fields are drawn in fig. 9.

To test the validity of the predictions embodied in eq. (5.6), Huppert and Worster [22] carried out a series of experiments in which aqueous solutions of $NaNO_3$, NaCl and NH_4Cl were cooled in the apparatus sketched in fig. 10. In each experiment, after a short initial period, the thickness of the solid block (ice) increased with the square root of time, as predicted by eq. (5.5). Four typical results for the measured growth rate eigenvalue λ_4 at different initial compositions C_∞ of $NaNO_3$ are plotted in fig. 11 and compared with the theoretical relationship [eq. (5.7)]. Agreement between the theoretical prediction and experimental data is seen to be totally absent.

The reason for the disagreement is that, under almost all conditions, the solid, in this case ice, does not grow with a stable planar interface. During solidification, solute is removed from the melt and a diffusion profile develops in that part of the melt that is adjacent to the interface between melt and solid. In the one-dimensional growth sketched in fig. 9 the relatively slow compositional diffusion, which is governed by the value of D ($\ll \kappa_\ell$ or κ_s), constraints the rate of growth of the interface. Instead, the interface in the experiments becomes highly irregular. (A photograph of the ice is reproduced as fig. 7 in Huppert [1].) The initial breakup of a planar interface is known as morphological instability, and discussed in detail in chapters 12–14. It suffices here to summarize the relevant results by stating that morphological stability was first considered at a qualitative level by Rutter and Chalmers [25]. They suggested that

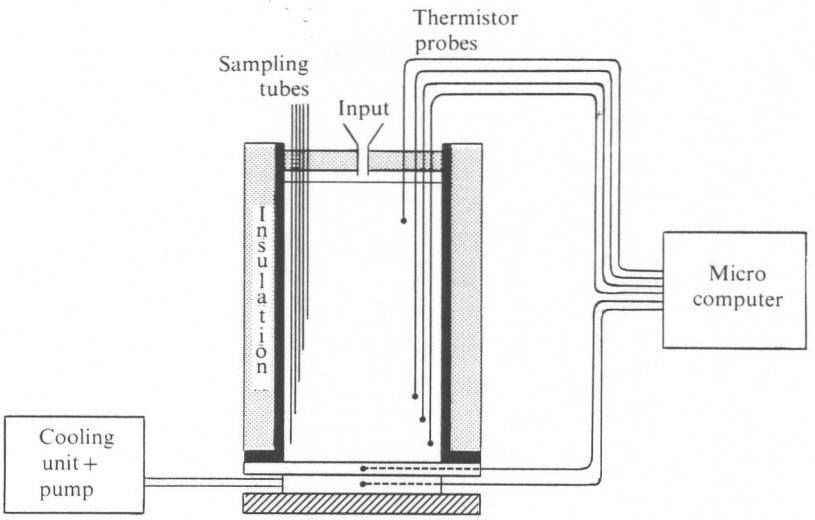

Fig. 10. Sketch of the apparatus used by Huppert and Worster [22] to cool and solidify various aqueous solutions.

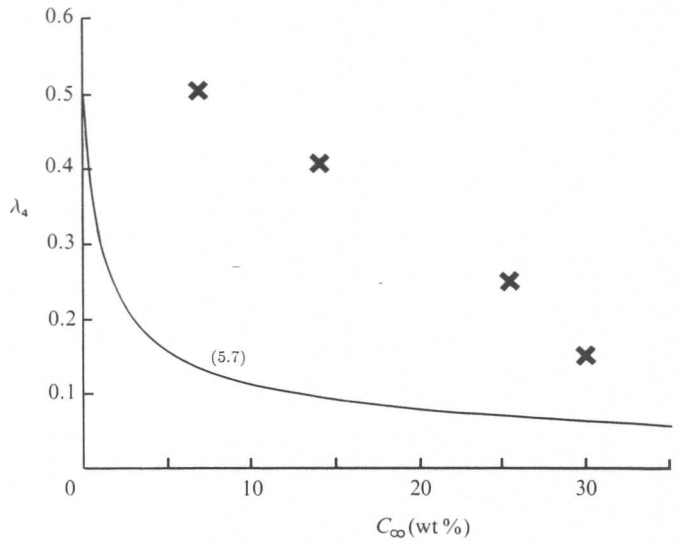

Fig. 11. The nondimensional growth rate λ_4 as a function of the initial far-field composition C_∞ for stable, one-dimensional solidification from below of aqueous $NaNO_3$, with $T_B = -17°C$ and $T_\infty = 15°C$. The solid curve represents the theoretical relationship (5.7) and the crosses represent the experimental data. The agreement is not impressive.

instability occurred whenever

$$-m_L \frac{\partial C}{\partial z} > \frac{\partial T}{\partial z} (>0) \quad (z = s(t) +) \tag{5.9}$$

because the temperature and composition fields predicted by the one-dimensional model on the melt side of the interface would then be below the liquidus, which implies

(inconsistently) that the melt is in the solid field. Quantitative dynamic calculations (but neglecting convective motions in the melt) were undertaken some years later by Mullins and Sekerka [26] to lead to the instability criterion.

$$-(K_s + K_\ell)m_L \left.\frac{\partial C}{\partial z}\right|_{s+} > K_s \left.\frac{\partial T}{\partial z}\right|_{s-} + K_\ell \left.\frac{\partial T}{\partial z}\right|_{z+} \tag{5.10}$$

if surface tension effects at the interface are ignored. This criterion reverts formally to eq. (5.9) if either K_s is set equal to zero or $K_s = K_\ell$ and $\mathscr{L} = 0$. Because the thermal and compositional fields are both stably stratified in the case we are currently considering, no convection can take place in the melt. This is in contrast to the case where the solidification releases light fluid, although numerical calculations incorporating the possibility of convection in the melt [27, 28] lead to results which, under usual conditions, differ little from either eq. (5.9) or eq. (5.10). A nice general review of the interaction between solidification and linear convection is presented in [29] and a section in [30] is also devoted to this topic. Further information can also be found in [31], which includes papers presented at a conference on the interaction between convection and solidification. All calculations indicate that only for very small values of both the undercooling $T_M - T_B$ and the resulting interfacial velocity ds/dt is the interface stable, as is presented quantitatively by Huppert and Worster [22] in their fig. 1. Paradoxically, no experiment has yet been performed that distinguishes between the slightly different predictions embodied in eqs. (5.9) and (5.10) and in the numerical calculations including the effects of linear convection in the melt. This reflects the fact that only for very special conditions will the planar interface be stable.

A physical explanation of the instability can be understood as an extension of the arguments already presented in section 3. As indicated in the sketch in fig. 12a, which presents the perturbed thermal and compositional fields, there are three competing effects: thermal fluxes, which are stabilizing; compositional fluxes, which are destabilizing; and surface energy effects, which again are stabilizing. The length scales associated with these are, respectively, $l_D = \kappa/V$, $l_C = D/V$, and $l_{GT} = \Gamma/\Delta T$, where l_D and l_{GT} have been defined in section 3 and D is the Fickian diffusion coefficient. Typically $l_{GT} \ll l_D \ll l_C$, which gives rise to a stability diagram of the form sketched in fig. 12b. If $\sigma > 0$ for any part of the dispersion relationship, as occurs for the dashed part of the curve in fig. 12b, the system is unstable to a *linear* perturbation. Equation (5.10) represents this condition analytically.

For many systems the inequality expressed in eq. (5.10) is exceeded significantly and it is not possible to describe the evolution of the system by linear theory or even by weakly nonlinear perturbations. Laboratory experiments of the sort described above indicate that the system actually departs significantly from one having a flat stable interface. Instead, a mushy region is formed in which interconnected solid is bathed in interstitial liquid. Mushy layers are such ubiquitous entities in solidifying systems that a considerable amount of the remaining part of this section will be devoted to determining and presenting the solutions of the governing equations that describe mushy layers.

Primarily motivated by their experimental results, Huppert and Worster [22] developed the following simple model for a mushy layer, which highlights many of the

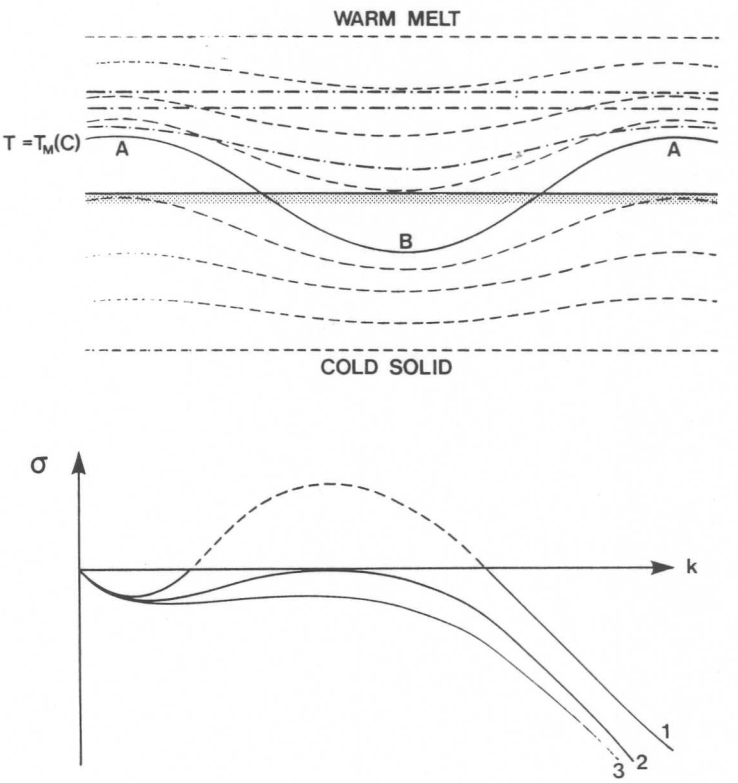

Fig. 12. (a) With the notation of fig. 4, a solid is advancing into a relatively warm two-component melt. The resulting curves of constant concentration in the melt are shown as dot-dashed curves. The enhanced compositional transfers near A induce extra solidification there, while the reduced compositional transfers near B induce less solidification there. The perturbed thermal transfers and surface tension effects lead to the opposite: extra solidification near B and less solidification near A. (b) The three effects which are discussed in the text and summarized in the caption to (a) lead to three possible dispersion relationships between the exponential growth rate σ and the wavenumber of the perturbation k. Curve 3 is totally stable; curve 2 is marginally stable; while for curve 1 a linear perturbation is unstable over the wavenumber range that is shown dashed.

important features. They postulated that the mush could be described by a constant solid fraction $\bar{\phi}$ and that global conservation equations, consistent with this idea, could be used to describe the transitions in the mushy layer. The resulting thermal and compositional fields are sketched in fig. 13. The temperature field satisfies

$$\frac{\partial T}{\partial t} = \bar{\kappa}\frac{\partial^2 T}{\partial z^2} \quad (0 < z \leqslant s(t)), \tag{5.11a}$$

$$\frac{\partial T}{\partial t} = \kappa_\ell \frac{\partial^2 T}{\partial z^2} \quad (s(t) < z), \tag{5.11b}$$

$$\mathscr{L}\bar{\phi}\frac{\mathrm{d}s}{\mathrm{d}t} = \bar{K}\frac{\partial T}{\partial z}\bigg|_{s-} - K_\ell \frac{\partial T}{\partial z}\bigg|_{s+}, \tag{5.11c}$$

where an overbar denotes values in the mush. These quantities are evaluated using

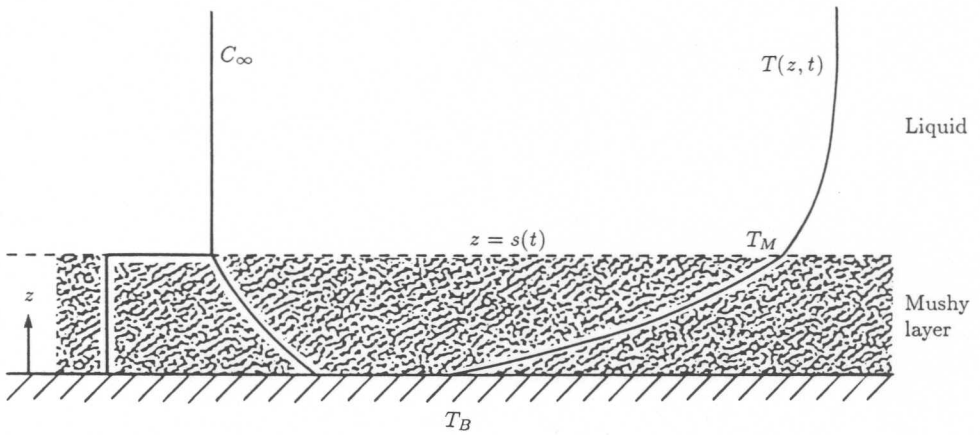

Fig. 13. Sketch of the temperature and composition profiles for a semi-infinite binary melt cooled from below to form a mushy layer on the release of liquid whose density exceeds that of the original melt.

averages weighted by the volume fraction to obtain

$$\bar{K} = \bar{\phi} K_s + (1 - \bar{\phi}) K_\ell = \bar{c}\bar{\kappa}, \tag{5.12a, b}$$

where

$$\bar{c} = \bar{\phi} c_s + (1 - \bar{\phi}) c_\ell . \tag{5.12c}$$

The representation (5.12a) is a good approximation for a random mixture of solid and liquid and becomes exact if the solid dendrites are of constant width and grow vertically [32] and is, therefore, a good approximation for diffusion-controlled growth in one dimension. Equation (5.12c) is always correct. In the mushy layer the composition is either zero in the solid dendrites or at the local liquidus in the interstitial melt, that is,

$$C = -T/m_L \quad (0 < z \leqslant s(t), \text{ within the interstitial melt}). \tag{5.13}$$

The composition field in the melt is negligibly influenced by the rapid growth of the mushy layer because of the relatively small value of the compositional diffusivity, and so

$$C = C_\infty \quad (s(t) \leqslant z). \tag{5.14}$$

Global conservation of solute requires that

$$(1 - \bar{\phi}) \int_0^{s(t)} C(z, t)\, dz = s(t) C_\infty . \tag{5.15}$$

In the model, conservation of solute is achieved by increasing the concentration of the melt within the interstices rather than pushing solute ahead of the advancing solidification front. The growth of solid is, thus, not constrained by the relatively slow molecular diffusion of composition, which is the cause of the instability of the planar interface.

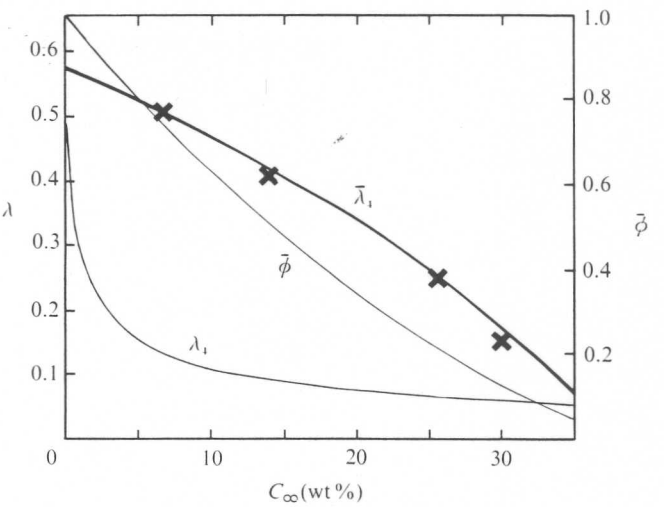

Fig. 14. The nondimensional growth rates λ_4 and $\bar{\lambda}_4$ [determined from eq. (5.17)] and the mean solid fraction $\bar{\phi}$ for solidification from below, with parameters as in fig. 11.

The system comprising eqs. (5.11)–(5.15), the boundary and initial conditions on the temperature field [eq. (2.3)] and the liquidus relationship [eq. (5.5)] applied at the tips of the dendrites [at $z = s(t)$] has the solution

$$s = 2\bar{\lambda}_4(\kappa_\ell t)^{1/2}, \tag{5.16}$$

where $\bar{\lambda}_4$ satisfies an equation of the form

$$F\left(\bar{\lambda}_4; \bar{\mathscr{S}}, \frac{c_\ell(T_\infty - T_L)}{\bar{c}(T_L - T_B)}, \frac{\bar{\kappa}}{\kappa_\ell}\right) = 0, \tag{5.17a}$$

with

$$G\left(\bar{\phi}; \frac{T_L}{T_B}, \frac{\bar{\kappa}}{\kappa_\ell}\right) = 0, \tag{5.17b}$$

while

$$\bar{\mathscr{S}} = \frac{\bar{\phi}\mathscr{L}}{\bar{c}(T_L - T_B)} \tag{5.18}$$

is the Stefan number across the mushy layer.

The predictions of the growth rate $\bar{\lambda}_4$ obtained by this approach are seen to agree well with the results of laboratory experiments using aqueous solutions, as is shown in fig. 14 for one particular series of experiments.

5.3. *Equations for mushy layers*

The good agreement between the data obtained from laboratory experiments and the simplest formulation of equations describing a mushy layer acted as a spur to develop

more general, but still easily solvable and interpretable, equations describing a mushy layer. With the assumption that the solid fraction $\phi(\boldsymbol{x}, t)$ within the mushy layer can change as a function for both space and time, it is relatively straightforward to derive conservation equations by considering "infinitesimal" control volumes which contain representative samples of both solid and liquid phases. With the neglect of density changes effects on solidification, convection in the interstitial liquid and with the assumption that the solid phase is fixed, and is not transported by the fluid as a slurry, the heat budget equation becomes

$$\bar{c}\frac{\partial T}{\partial t} = \nabla\cdot(\bar{K}\nabla T) + \mathscr{L}\frac{\partial \phi}{\partial t}. \tag{5.19}$$

This is a nonlinear diffusion equation, forced by the internal release of latent heat, which is proportional to the rate of change of the solid fraction. The corresponding compositional budget can be written as

$$(1-\phi)\frac{\partial C}{\partial t} = \nabla\cdot(D(1-\phi)\nabla T) + C\frac{\partial \phi}{\partial t}, \tag{5.20}$$

a(nother) nonlinear diffusion equation forced by internal release of solvent as ϕ varies with time. Further details on the derivation of these governing equations and the generalizations to allow for volume changes on solidification and convection can be found in Worster [3, 33].

The boundary conditions needed to solve eqs. (5.19) and (5.20) arise in two ways. The first ones reflect the prescribed conditions at the edge of the solution domain, and the second the conditions which describe the internal interfaces between either a solid and a liquid region or a mushy and a liquid region. Integrating eqs. (5.19) and (5.20) over a small pill box enclosing a portion of the interface (which is permissible because the equations are valid on both sides of the interface) and using the fact that both the temperature and the composition must be continuous across the interface, we obtain

$$\mathscr{L}[\phi]V = [\bar{K}\boldsymbol{n}\cdot\nabla T] \tag{5.21}$$

and

$$C[\phi]V = [D(1-\phi)\boldsymbol{n}\cdot\nabla C], \tag{5.22}$$

where [ ] denotes the jump in the enclosed quantity across the interface, which is assumed to be moving with normal velocity V and $\boldsymbol{n}$ is the unit normal vector.

The introduction of a first-order spatial derivative of ϕ into the mathematical model indicates that an additional interfacial condition on ϕ is required. A number of different conditions have been suggested, with Worster [33] advocating that the interface is at marginal equilibrium, with the normal derivative of the temperature at the mush–liquid interface being equal to the normal derivative of the local liquidus temperature. This condition is identical to the marginal stability criterion deduced by Rutter and Chalmers [25]. Mathematically, this condition can be expressed as

$$[\boldsymbol{n}\cdot\nabla T] = [\boldsymbol{n}\cdot\nabla T_{\mathrm{L}}] \equiv \frac{\mathrm{d}T_{\mathrm{L}}(C)}{\mathrm{d}C}[\boldsymbol{n}\cdot\nabla C]. \tag{5.23a, b}$$

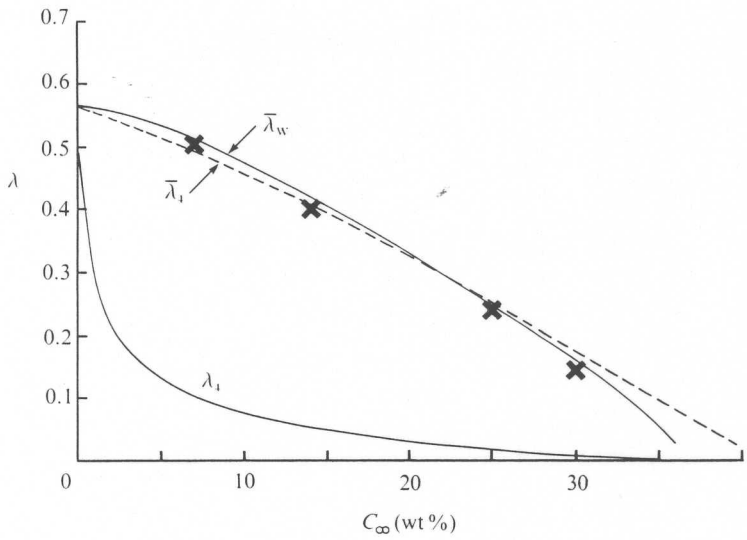

Fig. 15. The nondimensional growth rates λ_4, $\bar{\lambda}_4$ and $\bar{\lambda}_w$ (determined by Worster [33]), with parameters as in fig. 11.

In most circumstances eq. (5.23) implies that $[\phi] = 0$, or that $\phi = 0$ at an interface between a mushy layer and a liquid.

The validity of these concepts and equations can be partially tested by solving the equations for the problem outlined in the previous subsection. This was done by Worster [33], who found that because of the lack of an external length scale, the nonlinear equations had a solution in terms of a similarity variable $\eta = \frac{1}{2}z/(\kappa_\ell t)^{1/2}$, and that the top of the mush could, hence, be specified by

$$s = 2\bar{\lambda}_w(\kappa_\ell t)^{1/2}, \tag{5.24}$$

where $\bar{\lambda}_w$ is a function of the nondimensionalized external parameters. Figure 15 graphs the result for one particular set of parametric values and allows a comparison to be made both with $\bar{\lambda}_4$, obtained by the simpler method outlined above, and with the experimental data. The agreement with both is seen to be very good. Indeed, while the full model is intellectually much more satisfying, it does not seem to fit these particular observations significantly better than results from the simpler model. This suggests that such averaged models may have a useful role to play in more complicated situations.

A further test came from experimental measurements of ϕ by Shirtcliffe et al. [34], which were interpreted by them. Later, the data were reprocessed by Chiareli and Worster [35]. Measuring the conductivity of three vertically separated horizontal wires in a solidifying aqueous solution of sodium nitrate, Shirtcliffe et al. showed that the results were consistent with a similarity form of the solution and that they agreed fairly well with the explicit solution just outlined, as shown in fig. 16. Better agreement between theory and experiment, as also indicated in fig. 16, was found by Chiareli and Worster [35], who included in their theory the redistribution of solute due to the

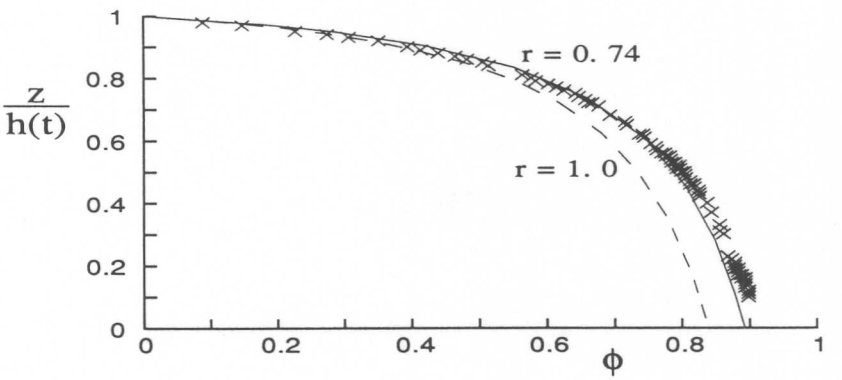

Fig. 16. The volume fraction of solid ϕ in a mushy layer as a function of the relative depth in the layer, $z/h(t)$, where $h(t)$ is the height of the layer. The data come from the experiments of Shirtcliffe et al. [34], using aqueous solutions of sodium nitrate. The dashed line is the prediction of a model that neglects changes in density upon solidification ($r \equiv \rho_s/\rho_\ell = 1$), while the solid line, taken from [35], takes full account of the interactions between solidification and the velocity field induced by shrinkage ($r = 0.74$).

change of density on solidification. As evident from fig. 16, this expansion introduces a change of approximately 10% in the prediction of the solid fraction.

There have been a number of approaches to the analysis of mushy layers which differ from the one outlined above. A very general thermodynamic approach to investigate the formation of both mushy layers and slurries has been commenced by Hills et al. [36]. They used the concepts of diffusive mixture theory to develop a set of rather complicated governing equations which incorporate much of the fundamental thermodynamics. Too few explicit solutions to the equations have yet been obtained to enable one to assess how applicable the model and the various approximations built into it are to the description of mushy layers. An extension to this approach, directed more explicitly at mobile slurries, has recently been presented by Loper [37, 38]. A different approach has been suggested by Bennon and Incropera [39] and the number of articles in Davis et al. [31] obtain numerical results employing their system of equations.

5.4. *Cooling from above a supereutectic binary alloy*

The validity of the mushy-layer equations (5.19)–(5.22) can be tested further, and additional fluid-mechanical effects can be investigated, by considering the solidification of a two-component layer of fluid that releases less dense fluid upon being cooled from above. The temperature will increase monotonically downwards throughout the solid (or mushy) layer and result in a potentially unstable thermal gradient in the liquid. Provided that the Rayleigh number of the liquid layer is above the critical value, the layer will convect. Further, this convection will be quite vigorous for sufficiently large values of the Rayleigh number. The resulting compositional gradient will be such that a mushy layer will form. Because the temperature increases with depth in the mushy layer and the interstitial liquid is assumed to be on the

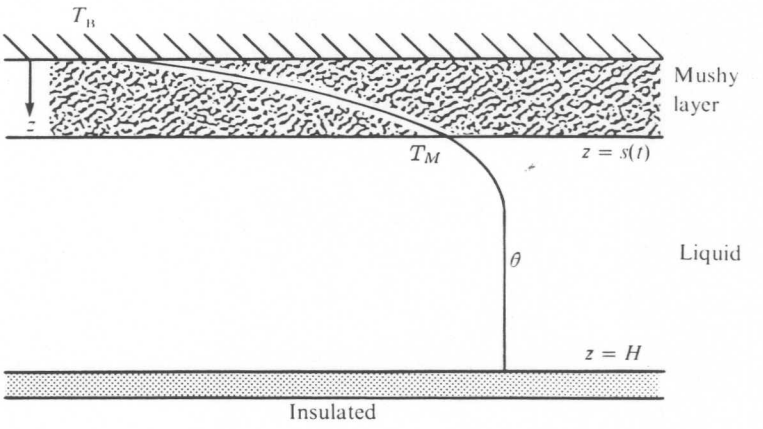

Fig. 17. Sketch of the temperature profile for a binary melt of initial depth H cooled from above to release melt whose density is less than that of the original melt.

liquidus, the density of the interstitial liquid is stably stratified and there are no convective motions in the mushy layer.

The resulting system is similar in many ways to the single-component system considered in section 4. The solid region of fig. 6 is replaced by a mushy region in fig. 17. The region of melt is modelled in the same way and its temperature obeys eq. (4.3a), with the heat flux given by eq. (4.3b), except that the solidification temperature T_M is replaced by the (unknown) temperature T_i of the interface between the mushy and liquid regions. If the diffusivity D of solute in the melt is small compared to the diffusivity κ of heat, as is typically the case, then the effects of the compositional boundary layer ahead of the mush–liquid interface are negligible and the interfacial temperature is given by

$$T_i = T_L(C_\ell) \quad (z = s), \tag{5.25}$$

where $T_L(C)$ is the liquidus temperature of the two-component system and C_ℓ is the composition of the melt. Equation (5.25) is the replacement of eq. (2.3b) and is appropriate under the assumption of local equilibrium. In the next subsection we shall consider a nonequilibrium growth law and discover important consequences of dis-equilibrium. For now we use the simpler condition of equilibrium thermodynamics in order to focus attention on effects related solely to a multicomponent, rather than a single-component, melt.

The equation expressing conservation of heat at the mush–liquid interface (4.4) is replaced by

$$\bar{K} \left.\frac{\partial T}{\partial z}\right|_{s^-} = F_T + (T_\ell - T_i)\frac{ds}{dt}, \tag{5.26}$$

where $z = s$ is the position of the mush–liquid interface. Note that there is no release of latent heat at this interface since the solid fraction in the mushy layer there is zero when $D/\kappa \ll 1$ and thermodynamic equilibrium is assumed. Instead, the release of latent heat is distributed throughout the mushy layer as expressed by the nonlinear

thermal-diffusion equation (5.19), which in this case takes the form

$$\bar{c}\frac{\partial T}{\partial t} = \frac{\partial}{\partial z}\left(\bar{K}\frac{\partial T}{\partial z}\right) + \mathscr{L}\frac{\partial \phi}{\partial t}. \tag{5.27}$$

An additional equation is required to determine how the solid fraction varies within the mushy layer. Since the microstructure of the mushy layer is so fine and the relative surface area of phase boundaries within the layer is consequently so large, it is a very good approximation to assume that

$$T = T_{\mathrm{L}}(C) \tag{5.28}$$

within the layer, i.e., the mushy region is in local thermodynamic equilibrium. The concentration C of the interstitial liquid is found, by conservation of solute from eq. (5.20), to satisfy

$$(1-\phi)\frac{\partial C}{\partial t} = (C - C_{\mathrm{s}})\frac{\partial \phi}{\partial t}, \tag{5.29}$$

where C_{s} is the (uniform) concentration in the solid phase and we have ignored the diffusion of solute because $D \ll \kappa$.

Appropriately nondimensionalizing these governing equations [18, 40] introduces the parameter

$$\mathscr{C} = \frac{C_{\mathrm{s}} - C_0}{C_0 - C_{\mathrm{B}}}, \tag{5.30}$$

where C_0 is the initial concentration of the melt and $T_{\mathrm{L}}(C_{\mathrm{B}}) = T_{\mathrm{B}}$. The parameter $\mathscr{C}$ represents the difference in composition between the solid and liquid phases relative to the variations in concentration of the liquid phase within the mushy layer. The value of $\mathscr{C}$ is zero for a pure melt and is always positive otherwise. In this system of equations, the Stefan number $\mathscr{L}/c_{\ell}[T_{\mathrm{L}}(C_0) - T_{\mathrm{B}}]$ only appears divided by $\mathscr{C}$. Thus positive values of $\mathscr{C}$ serve to reduce the effective value of the Stefan number.

Numerical solutions of the resulting equations were obtained by Kerr et al. [40]. They also carried out a series of experiments with aqueous isopropanol (with C_0 around 17 wt% isopropanol), which led to the formation of ice and the release of an isopropanol-enriched solution. Both the ice and the released solution were less dense than the original solution. Thus, a relatively light mushy ice layer, bathed in stagnant, isopropanol-enriched water, formed at the top of the container. This cold layer maintained turbulent thermal convection in the fluid below.

A comparison between the theoretically and experimentally obtained results is presented in fig. 18, where the appropriate theoretical curve is the one marked "equilibrium". The agreement between the theoretical predictions and the experimental data for both the position of the interface and the temperature of the melt appears to be good. However, one notices that the measured temperature of the aqueous isopropanol was always below the predicted temperature, and, after approximately 300 min, was also below the liquidus temperature – and by a fairly significant amount ($\sim 1^{\circ}$C). This signifies that the melt must become locally supersaturated in

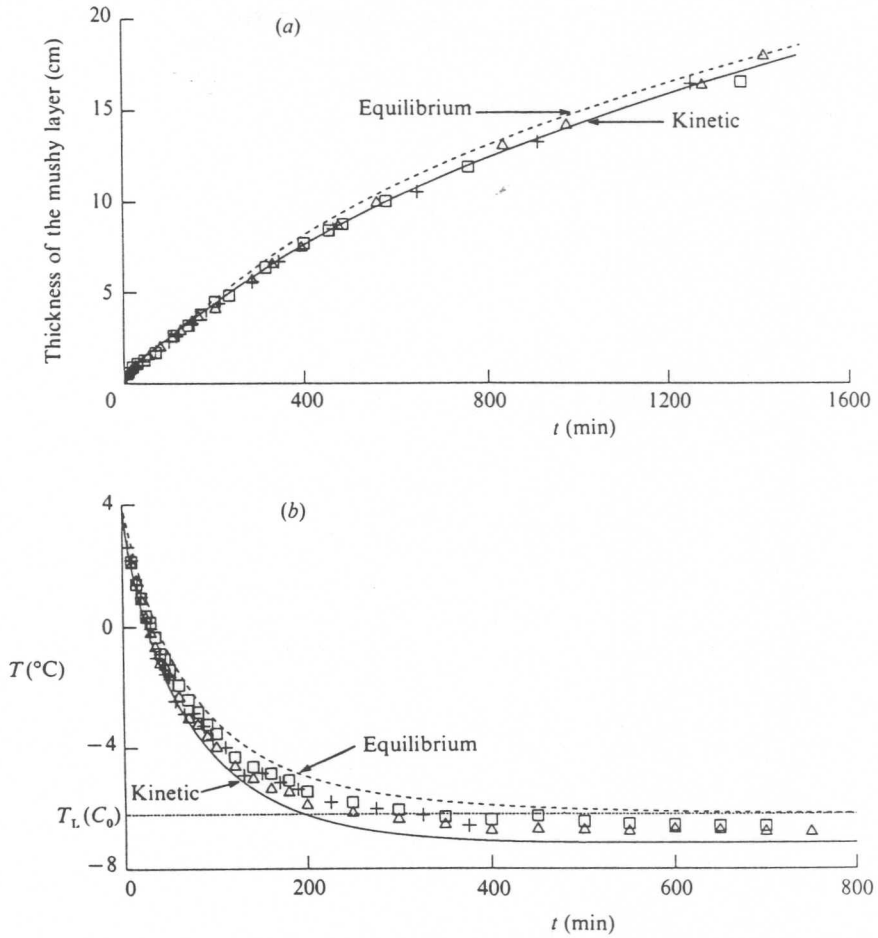

Fig. 18. (a) The thickness $s(t)$ of the mushy layer and (b) the temperature T of cooled aqueous isopropanol as functions of time. The dashed curves are the result of a theoretical model based on the assumption of thermodynamic equilibrium and the solid curves incorporate the kinetic growth law [eq. (5.31)]. The symbols represent the data from different experiments in which $C_0 = 83.2$ wt% H_2O, $T_0 = 4.0°C$, $T_B = -17°C$ and $H = 18.8$ cm.

order for solidification to occur. We, thus, describe the incorporation of the concept of supersaturation into a model which relaxes the assumption that solidification occurs at thermodynamic equilibrium. Aside from leading to better agreement with the experimental data, the predictions of the model have far-ranging consequences, which include the conditions under which large bodies of melt, such as the molten rock (magma) contained in storage reservoirs within the Earth, can convect when cooled from above [41].

Nonequilibrium processes of crystal growth can be modelled by incorporating the concept that, away from thermodynamic equilibrium, the rate of growth of solid is directly related to the value of the local supersaturation. This concept has a rather broad and old foundation (see, e.g., [42] for a general survey and [43] for an explicit application which has some similarities with that presented here). Experiments with

aqueous isopropanol suggest the simple linear relationship [44]

$$\frac{ds}{dt} = \mathscr{G}(T_L - T_i) \quad (z = s(t)), \tag{5.31}$$

with $T_i < T_L$, where T_L is the liquidus temperature at the interface, T_i is now the *unknown* solidification temperature at the interface and $\mathscr{G}$ is an empirical constant, determined for aqueous isopropanol to be $2.2 \times 10^{-4}\,\mathrm{cm\,s^{-1}\,^{\circ}C^{-1}}$ [44]. More complicated, nonlinear relationships, for different substances, reflecting the different styles of growth of individual crystals, have been suggested, but eq. (5.31) represents a good fit to the experimental data for aqueous isopropanol.

The result of incorporating eq. (5.31) into the numerical simulation of the experiments is shown labelled "kinetic" in fig. 18. The theoretical predictions for the position of the solidification front are seen to be in excellent agreement with the experimental data. Those for the temperature of the melt satisfactorily account for the occurrence and time of initiation of the supersaturation but are slightly less than the observed temperatures. It is believed that the observed temperatures may have been slightly increased by heat gains from the laboratory.

The fact that in the interior the melt was at a temperature below its liquidus temperature, and was, hence, supersaturated suggests that had there been nucleation sites for crystallization within the melt, there could have been growth additional to that which occurred in the mushy layer. This was not so in experiments with aqueous isopropanol because the solid ice crystals were lower in density than the original melt and nucleation was not observed in the interior of the solution. On the other hand, experiments with aqueous sodium sulphate formed relatively heavy sodium sulphate decahydrate crystals, some of which settled to the base of the tank, leading to growth of solid at the floor. This illustrates the important concept that, under suitable conditions, cooling at the roof of a container leads to crystallization at the floor remote from the site of cooling, as observed previously by Turner et al. [17] and described by Brandeis and Jaupart [45]. A description of the theoretical model we developed to account for the growth on the floor is presented in the next subsection.

5.5. Compositional stratification in the solid

Stratification of composition in the solid, or zoning as geologists sometimes call it, that results from solidification of a multicomponent melt is important in many different situations. For it to result from a two-component melt, it is necessary that solidification of both component end-members occurs. This can result from variation of composition along the solidus, although this is generally a small effect. Indeed, for most aqueous solutions it is totally absent. More generally, compositional stratification can arise only if cooling takes place below the eutectic temperature T_E, the minimum temperature at which the melt can remain liquid, at least at thermodynamic equilibrium.

With the geometry considered in the last subsection, compositional stratification will result if T_B is maintained below T_E. In this case the thermal profile is as sketched

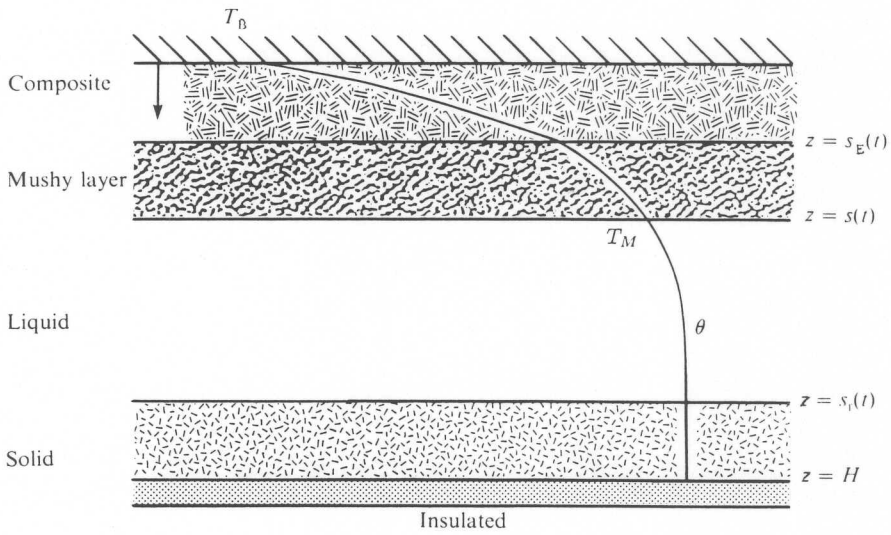

Fig. 19. Sketch of the temperature profile for a binary melt of initial depth H cooled from above to release melt whose density is less than that of the original melt, with the boundary maintained at a temperature that is below the eutectic temperature.

in fig. 19. Commencing from the roof, the first layer, which occupies $0 < z \leqslant s_E(t)$, consists of a composite solid made up of crystals of the two pure end-members. The temperature at the boundary $s_E(t)$ is the eutectic temperature T_E. Heat is transferred by conduction through this layer and, once the solid is laid down, the composition is independent of time. Beneath this solid layer there is a stagnant mushy layer, just as before, which occupies $s_E(t) \leqslant z \leqslant s(t)$. The layer between $z = s(t)$ and $z = s_f(t)$ is occupied by the turbulently convecting melt which transfers heat into the mushy layer. Finally, in $s_f(t) \leqslant z < H$, secondary crystallization leads to a solid layer growing from the floor. With time, the eutectic front at $z = s_E(t)$ reaches the solid layer growing from the floor and the solidification is complete.

A series of experiments were conducted by Kerr et al. [46, 47] using aqueous sodium sulphate in order to investigate this situation. The results of the experimental observations and the theoretical predictions, using the fitted value of $\mathscr{G} = 1.5 \times 10^{-4}\,\mathrm{cm\,s^{-1}\,^{\circ}C^{-1}}$ for aqueous sodium sulphate, are shown for a typical experiment in fig. 20. Figure 20a indicates that the thickness of each of the three layers that are either partially or totally solid grew with time, in good agreement with the theoretical predictions. From fig. 20b we see that there is a good agreement between the theoretical curves and experimental data for the temperature of the melt as a function of time. For comparison, we also present the liquidus temperature at the initial concentration. The mean composition in the composite layer decreased with depth from the roof, as is depicted in fig. 20c, owing to the gradual decrease in composition of the melt throughout the experiment. There is a discontinuity in the mean composition at the height where the downward-growing mushy layer met the upward-growing crystal layer from the floor. The measured compositional profile was fairly well predicted by the theory.

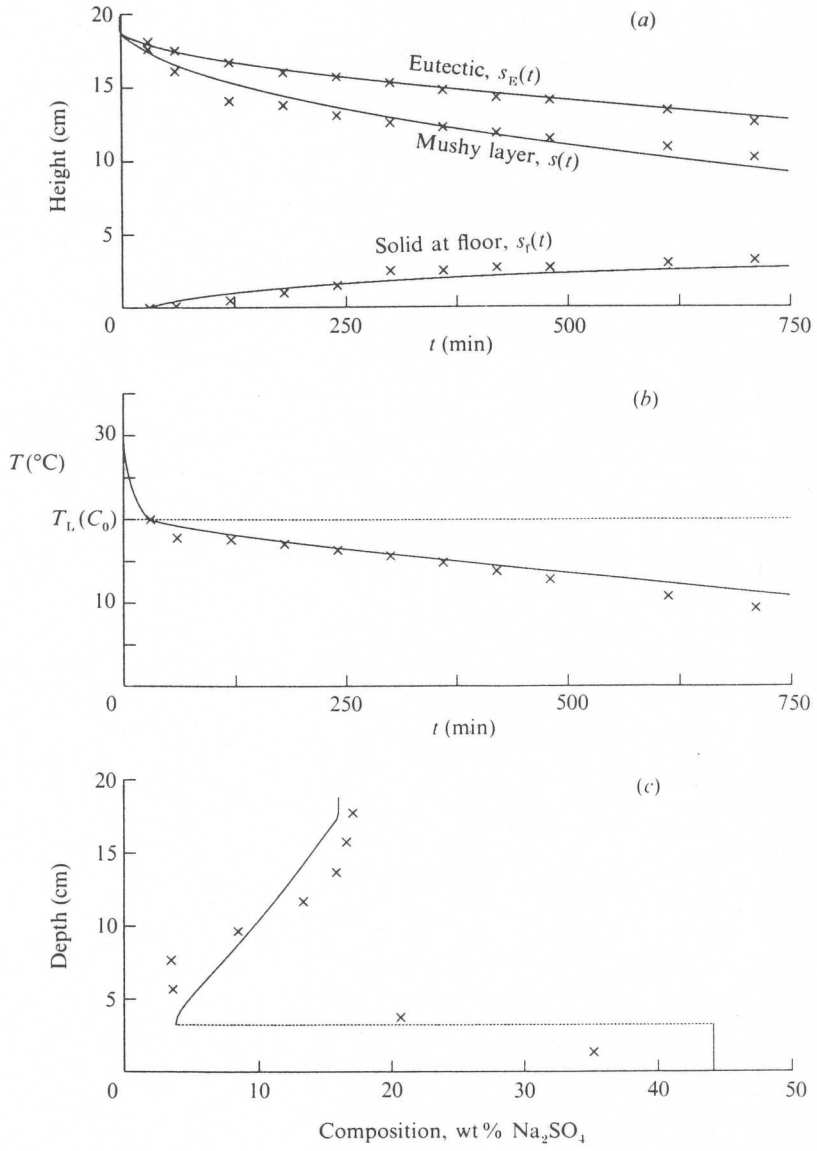

Fig. 20. The predicted results and the experimental data for cooling an aqueous solution of Na_2SO_4 from above for the same values of the physical parameters as in fig. 19: (a) height of the three interfaces as functions of time; (b) temperature of the liquid as a function of time; and (c) composition of the final solid product as a function of depth.

A more complicated situation arises and new concepts are introduced on consideration of the cooling from below of a melt that releases less dense fluid on solidification. If the appropriate compositional Rayleigh number is sufficiently large, as we shall assume, compositional effects in this case lead to vigorous mixing of the melt. Aside from the compositional transfers associated with this mixing, there are important thermal transfers to which the compositional transfers are coupled. The coupling arises because the compositional flux determines the intensity of the convective motions in the melt, which in turn determines the thermal flux. This flux regulates the

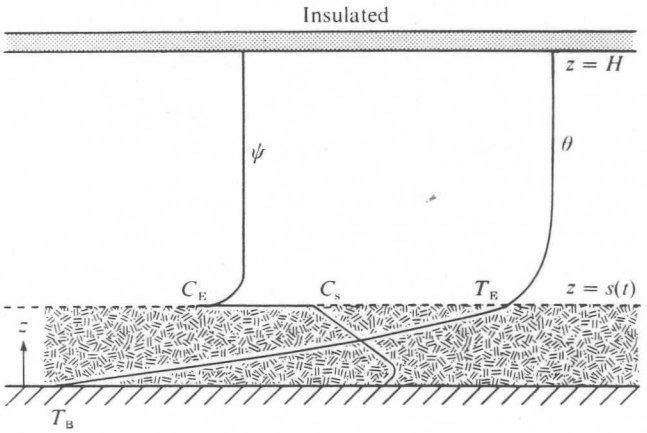

Fig. 21. Sketch of the temperature and composition profiles for a binary melt of initial depth H cooled from below to release melt whose density is less than that of the original melt with the boundary maintained at below the eutectic temperature.

solidification rate and, thus, the rate at which less dense fluid is released, i.e., the compositional flux. Part of the aim of an investigation by Woods and Huppert [49] was to study the relationship between the compositional flux from, and the thermal flux towards, the interface between melt and solid.

The geometry of their model and the generated profiles of temperature and composition are depicted in fig. 21. For the sake of simplicity, they neglected all effects due to nonequilibrium thermodynamics and to the formation of a mushy layer at the top of the crystal pile. Neglecting the latter was an outcome of experiments with aqueous Na_2CO_3, for which the observed mushy layer was only of order 1 mm thick. An investigation of the structure of such a mushy layer, the conditions under which it will form and the convection induced within it is presented in [3, 48].

The compositional flux F_c was determined by assuming that the four-thirds law of turbulent thermal convection [cf. eq. (4.3)] can be suitably modified to cover turbulent compositional convection by writing

$$F_C = \gamma_c c(g\beta D^2/\nu)^{1/3}\Delta C^{4/3}, \tag{5.32}$$

where β is the fractional increase in melt density per unit increase in composition, ΔC the compositional change across the compositional boundary layer on top of the solid layer and γ_c an empirical constant which may be different from γ because of the different boundary conditions on heat and composition. Since the turbulent intensity drives both the thermal and compositional transfers, the nondimensional heat flux, or thermal Nusselt number, $F_T H/c\kappa\Delta T$, associated with the compositional flux, will be linearly proportional to the compositional Nusselt number $F_C H/cD\Delta C$. The functional relationship, however, may possibly involve the Prandtl number and the ratio of the thermal and compositional diffusivities as well as whether the melt is undersaturated or saturated, since for the latter the temperature and composition in the

melt are coupled by the liquidus relationship. Mathematically, this means that

$$F_T = f\left(\frac{\kappa_\ell}{D}, \frac{v}{\kappa_\ell}\right)\left(\frac{\Delta T}{\Delta C}\right) F_C, \tag{5.33}$$

where f may depend not only on the explicit parameters displayed but also on whether the melt is saturated or undersaturated. When the melt is saturated $\Delta T = m_L \Delta C$ if the liquidus relationship is assumed to be linear. Woods and Huppert [49] also present three tentative physical models of the behaviour of the boundary layer at the interface which suggest explicit formulae for f.

The governing equations can then be formulated as follows. Within the solid, the temperature field satisfies the linear equation of heat conduction. However, in order to simplify the analysis, they replaced this with the linear temperature profile [c.f. eq. (2.10)].

$$T(z, t) = T_B + (T_E - T_B) z/s(t). \tag{5.34}$$

This is a good approximation to the full solution of the heat conduction equation provided that effects due to thermal conduction propagate more rapidly than does the interface between melt and solid. That is, provided $s \ll (\kappa_m t)^{1/2}$. This inequality is generally well satisfied (see, e.g., [17, 50]). The incorporation of eq. (5.34) greatly simplifies the analysis because the remaining equations are then all ordinary differential equations in time and no partial differential equations need be solved. At the interface between the melt and the solid, conservation of heat requires that [cf. eq. (4.4)]

$$k_s(T_E - T_B)/s = f J_c(\theta - T_E)(\psi - C_E)^{1/3} + [c_\ell(\theta - T_E) + \mathscr{L}]\frac{ds}{dt}, \tag{5.35}$$

where ψ and C_E are the composition of the melt and the eutectic, respectively, and $J_c = \gamma_c(g\beta D^2/v)^{1/3}$, while conservation of matter requires that

$$(C_s - \psi)\frac{ds}{dt} = J_c(\psi - C_E)^{4/3}, \tag{5.36}$$

where C_s is the composition of the solid. Within the melt, the thermal balance can be written as [cf. eq. (4.3)]

$$(H - s)\frac{d\theta}{dt} = -f J_c(\theta - T_E)(\psi - C_E)^{1/3}, \tag{5.37}$$

while conservation of matter requires that

$$(H - s)\frac{d\psi}{dt} = -J_c(\psi - C_E)^{4/3}. \tag{5.38}$$

The system for the four unknowns θ, ψ, C_s and s represented by eqs. (5.35)–(5.38) is subject to the initial conditions

$$\theta = T_0, \qquad \psi = C_0, \qquad C_s = C_0, \qquad s = 0 \quad (t = 0), \tag{5.39}$$

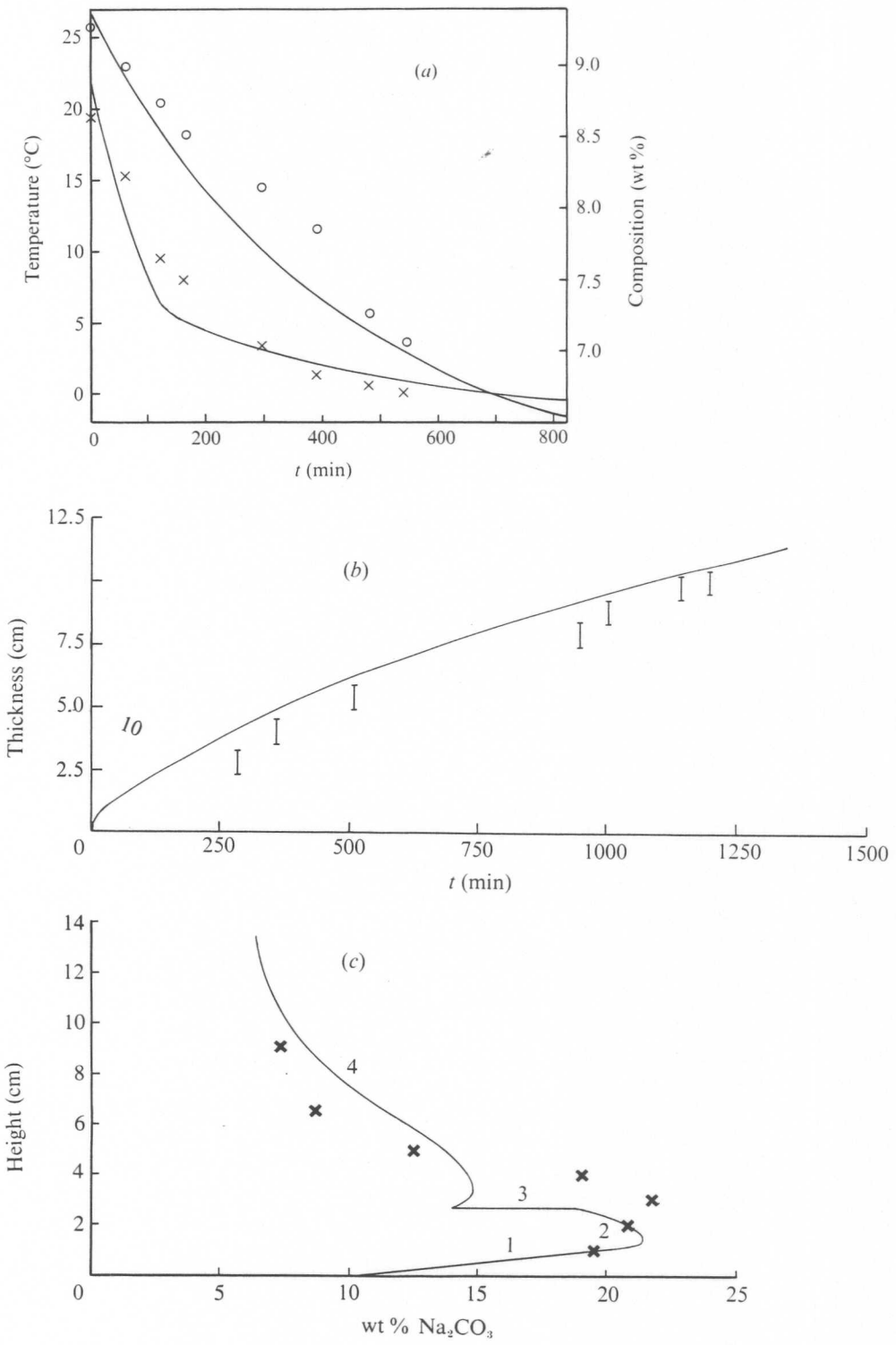

Fig. 22. The predicted results and experimental data for cooling an aqueous solution of Na_2CO_3 from below, with $C_0 = 9.34$ wt% Na_2CO_3, $T_0 = 19.4°C$, $T_B = -20°C$ and $H = 22$ cm: (a) Temperature and composition in the liquid as functions of time; (b) thickness of the solid layer as a function of time; and (c) composition of the final solid product as a function of depth.

where T_0 and C_0 are, respectively, the initial temperature and concentration of the melt. Equations (5.35)–(5.39), with the one free parameter f, can be integrated numerically (either with or without suitable nondimensionalization) to lead to theoretical predictions against which laboratory data can be compared.

Experiments with aqueous sodium carbonate, with a fixed value of κ_m/D and ν/κ_m, indicated that the data were best fitted by taking $f = 3$ when the melt was undersaturated and $f = 1$ when saturated. The results of a particular integration of eqs. (5.35)–(5.39) are graphed in fig. 22 and compared there with laboratory data. In fig. 22a, b, which present comparisons for temperature and composition in the melt and the height of the solid as functions of time, the agreement between theory and experiment is quite good. The agreement in fig. 22c, which presents the composition of the solid as a function of depth, is not as good, but still quite reasonable. The various segments in the theoretical curve indicate the different fluid regimes under which the solid was formed. For $s < 2.4$ cm ($t < 150$ min) the melt was predicted to be undersaturated. Beyond these limits, saturation was predicted. The various segments of the theoretical curve of fig. 22c took up different shapes, depending upon the relative balance between the convective and latent heat terms on the right-hand side of eq. (5.35). For most of the segment labelled 1, latent heat was dominant. With time, its relative effect weakened, which lead to the decrease of the composition of the solid with height as convective effects became dominant along the segment marked 2. At the end of this, the melt became saturated, at which point the model (discontinuously) reduced f from 3 to 1 along the segment marked 3. In reality, f will change more gradually and nonequilibrium effects will also occur, which explains the lack of agreement between theory and experiment at this point. The concentration of the solid thereafter adjusted rather rapidly at first to accommodate the discontinuity in the model. Subsequently, along the rest of the segment marked 4, the concentration in the solid decreased slowly as the temperature and concentration of the melt decreased.

6. *Solidification from a vertical wall*

Cooling and crystallizing a melt from a vertical side-wall requires a second spatial dimension to be considered because horizontal thermal and compositional gradients interact with the predominantly vertical flow of released fluid due to the vertical orientation of gravity. The situation of pure cooling (or heating) without crystallization at a semi-infinite wall is by now a classical problem in fluid mechanics (see, e.g., [51, 52]). The inclusion of crystallization adds two new effects. One is due to the presence of compositional influences in addition to thermal influences, and the other is due to the moving boundary between solid and melt. The incorporation of both these effects together has so far resisted analytical investigation, although a number of numerical investigations have considered this situation. On the assumption that the effects of crystallization can be treated by specifying a thermal and compositional anomaly at the (fixed) wall, and, hence, neglecting the solid regime that is formed, a number of authors have presented boundary layer analyses of flow past a vertical wall in an infinite fluid [53–56].

All these studies have focused on the situation for which the density anomaly at the wall due to temperature, $\Delta\rho_T$, is positive, which corresponds to a cooled wall and by itself would induce downwards motion, while the density anomaly at the wall due to composition, $\Delta\rho_C$, is negative, which corresponds to the release of less dense fluid and by itself induces upwards motion. Part of the reason that this situation has received maximum attention is because it is the one most relevant to a geological context. It is also the one that arouses most fluid-mechanical interest because of the inherent possibility of a bidirectional boundary layer. In the limit $D \ll \kappa \ll \nu$, three separate boundary layer regions can be discerned. In the inner region, which is closest to the wall, compositional buoyancy forces due to compositional differences balance viscous forces. Beyond this, in an intermediate region, buoyancy forces due to thermal differences balance viscous forces. Finally, in the furthest region, the inner and intermediate motions are responded to by viscous coupling with the inertia forces. The flow and relative strengths of the boundary layers depend on only three external parameters: the Prandtl number $Pr = \nu/\kappa$; the ratio of the diffusivities $\tau = D/\kappa$; and the (positive) ratio $r = -\Delta\rho_T/\Delta\rho_C$. For sufficiently small r, compositional effects overpower thermal effects and the entire flow is predicted to be upwards. For sufficiently large r thermal effects dominate and the entire flow is downwards. For intermediate values of r, a bidirectional motion results, with an upwards inner flow and a downwards intermediate flow. For large Pr, Nilson [55] showed that the bidirectional flow occurred whenever $0.62\tau < r < 1.09\tau^{1/3}$. On the further assumption that $\tau \ll 1$, as is typically the case, Nilson used asymptotic expansions to match the inner upwards-flowing boundary layer, whose width increased as $x^{1/4}$, where x is the distance from the base of the wall, to the very much thicker downwards-flowing boundary layer, whose width increased as $(L - x)^{1/4}$, where L is the total length of the wall. A typical example of the resulting self-similar vertical velocity, adapted from Nilson et al. [56], is drawn in fig. 23.

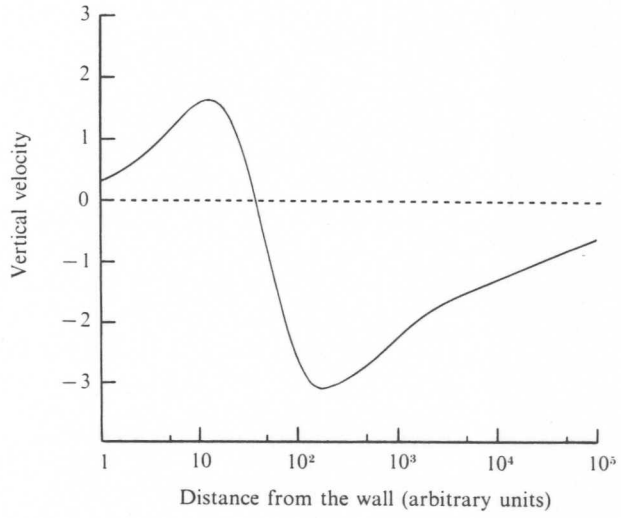

Fig. 23. The self-similar vertical velocity as a function of distance from a wall which is maintained at a decreased temperature and an increased composition over the far-field value.

A similar calculation, assuming that the flow takes place in a porous medium, has been conducted by Lowell [57], who also suggests that the value of r determines whether the flow is all upwards or all downwards or takes place in a bidirectional boundary layer. Such bidirectional boundary layer flows are fairly easy to set up and to visualize in a laboratory experiment.

These analytical calculations have all assumed that the ambient conditions far from the wall are constant. If the wall is part of a container, the boundary layer flows alter the environment and, in turn, are altered by it. This brings about new phenomena. Some of these have been investigated from an experimental point of view (see, e.g., [58–63]), while the work of Thompson and Szekely [64, 65], was one of the first theoretical studies. The latter authors also conducted laboratory experiments with

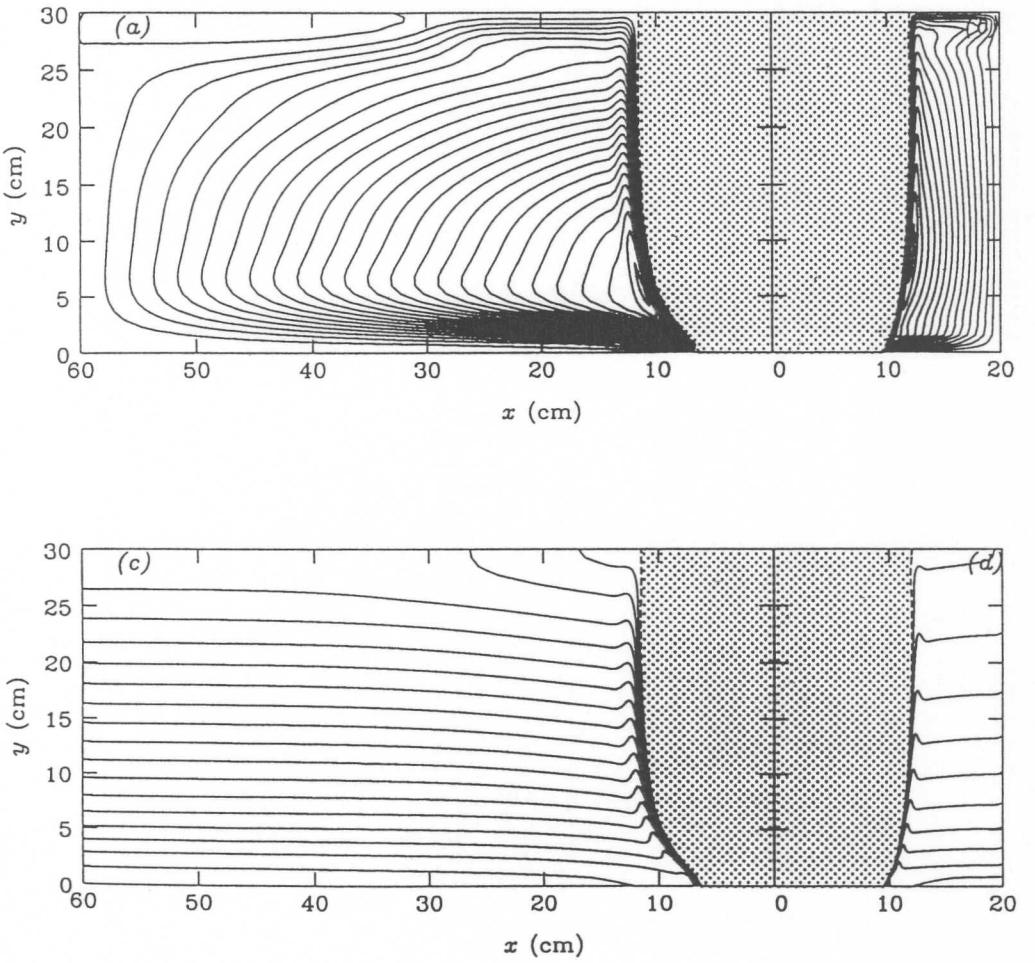

Fig. 24. Numerically calculated two-dimensional streamlines and liquid composition after 24 h for the partial crystallization of a stratified supereutectic aqueous solution of sodium carbonate for (a), (c) a tank 60 × 30 cm high, and (b), (d) a smaller tank 20 × 30 cm high. The cold boundary at $x = 0$ was maintained at a temperature of -21.5°C. The initially uniform temperature in both tanks was 15.5°C and the initial composition varied linearly from 13.0 wt% Na_2CO_3 at the base to 6.2 wt% Na_2CO_3 at the top in accord with experiments reported in [74]. The calculations are further explained in [71].

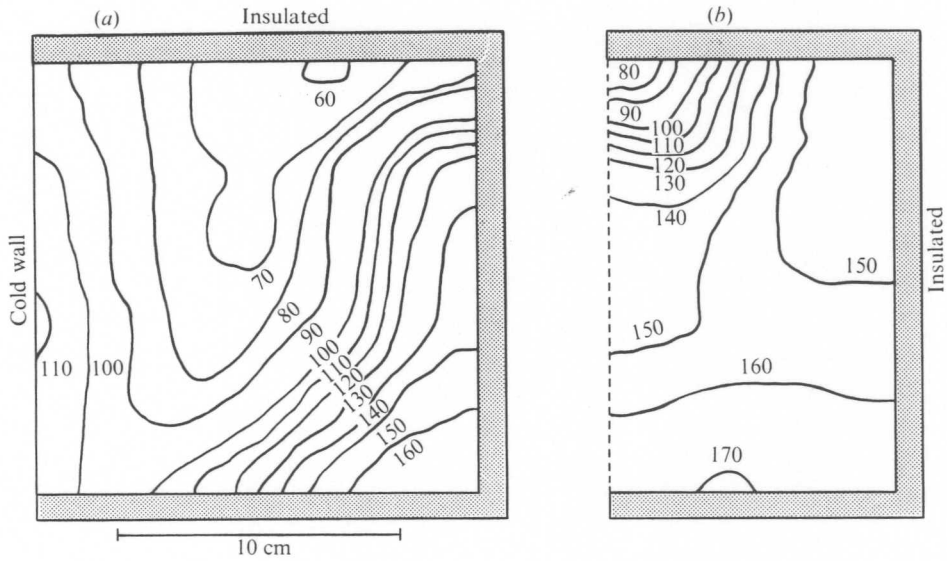

Fig. 25. The distribution of composition, in units of kg of $Na_2CO_3 \cdot 10H_2O$ per m^3 of solution, in the solid product obtained by cooling an initially homogeneous aqueous solution of Na_2CO_3 at a vertical wall. The initial composition was 111 kg of $Na_2CO_3 \cdot 10H_2O$ per m^3 of solution: (a) concentration in the middle plane of the tank, parallel to two insulated sides; (b) concentration in half the transverse section at the insulated end of (a).

which to compare their numerical calculations. Further numerical calculations have been summarized by Amberg [66], who has tried to identify the important external parameters and use these to collapse in a systematic way the output from different calculations and experiments. Reviews of some of these calculations are presented in the papers by Amberg, Voller and Schneider and Beckermann that appear in [31].

The major conclusion of all these studies is that solidification from the side of an initially homogeneous solution results in the formation of a vertical composition gradient in the melt. The gradient results from the convection driven by the fluid released on solidification, whether it be more or less dense than the original fluid. Cooling a vertical compositional gradient from the side leads to an array of nearly horizontal double-diffusive layers separated by sharp interfaces, as described by Huppert and Turner [67] and by Huppert et al. [68]. (Interested readers will find a description of the fundamental processes of double-diffusive convection, or thermosolutal convection as it is sometimes called, in [69, 70] and the references therein.) Figure 24 is one of the results of the extensive numerical calculations, performed by Jarvis [71]. The initial development of double-diffusive layers in the calculations is becoming evident, but more computer time would be needed to simulate the further evolution.

Aside from the stratification set up in the fluid, there is also compositional stratification in the resulting solid product. In her dissertation, Leitch [62] extended the earlier pioneering work of Turner and Gustafson [60] to discuss experiments in which initially uniform solutions of aqueous sodium carbonate were cooled from a sidewall

of a tank $16 \times 20 \times 15$ cm high. The refrigeration unit that provided the coolant was operated at its maximum power; thus, the temperature of the cold wall was not controlled (although it was recorded). The resulting distribution of composition in the solid, measured at the end of the experiment for which the initial concentration of Na_2CO_3 was less than the eutectic value, is shown in fig. 25. Considerable spatial variations in composition, both in the horizontal and in the vertical directions, are clearly evident, although these variations are not yet quantitatively understood. Similar variations in the resulting solid composition were reported by Hebditch [72], who solidified melts composed of lead and tin by cooling them at a vertical wall. The broad similarity between the results of these two sets of experiments indicate that the phenomena seen in aqueous salt solutions are replicated in other fluids with widely different properties.

7. *Crystallization on a slope*

Many of the principles enunciated in the previous sections are displayed in the study of crystallization resulting from cooling at a slope. In a series of experiments Huppert et al. [73, 74] inserted a cooling plate at an angle to the vertical into the interior of an aqueous solution. A particularly illustrative case is that in which the slope is at 45° to the vertical and is inserted symmetrically into the container. The slope then divides the fluid into two geometrically indentical regions. If convective effects were absent, solidification would proceed identically in the two regions. However, the influence of convection was observed to be dominant, although different, in the two regions.

Some of the experiments used an initially homogeneous solution of sodium carbonate whose concentration was greater than the eutectic value. In both regions, less dense fluid was released by the crystallization on the upper and lower surfaces of the cooling plate. Above the plate, the released fluid was free to rise and did so in a series of plumes, which mixed with the environment to produce a complicated large-scale flow.

Part of the flow consisted of strong motions up the slope of fluid from the interior entrained into the boundary layer and drawn towards the sites of crystallization. Another part of the flow was driven by the horizontal density gradients set up by the different heights of the plumes and, hence, different amounts of mixing along the slope. The released fluid which formed below the plate, on the other hand, was not free to rise because of the constraint of the overlying plate. The fluid slowly migrated through the crystal mush and was deposited at the top of the layer. Because of the cooling, the temperature of the interior decreased with time and, so, the density of the released fluid decreased also, in accord with the phase diagram of fig. 8b. Thus, newly released fluid flowed to the top of the region and displaced downwards the fluid previously deposited there, just as in the now classical "filling-box" situation [75–77]. As in that situation, the sharp interface between the released fluid and the initial fluid propagated downwards and a quite strongly stratified, virtually stagnant fluid region evolved above the interface. The macroscopic crystal structure took three forms: above the slope there was a very smooth interface between the crystals and the fluid

due to the strong up-slope motions in the latter; in the lower part of the downwards-facing surface, the interface was fairly convoluted owing to the fluid being irregularly crystallized at randomly oriented nucleation sites, while in the upper part of the surface there were much longer crystals and a more convoluted interface. With time, the interface in the region below the slope reached the bottom and eventually all the remaining fluid was at the eutectic composition. In the region above the slope, horizontal thermal and compositional gradients induced the ubiquitous double-diffusive layering and strong velocity gradients.

Experiments which commenced with a vertical gradient of composition [74] showed again that vertical density gradients have a strong restraining influence on compositional convection. A series of double-diffusive layers evolved, with thin plumes only occasionally penetrating one of the interfaces. Owing to the large molecular diffusivity of heat in comparison with that of composition, the circulation in the double-diffusive layers was controlled by thermal effects, even in regions where the plume motion due to compositional convection partially opposed the sense of motion. The compositional variations in the solid resulting from one experiment are shown in fig. 26.

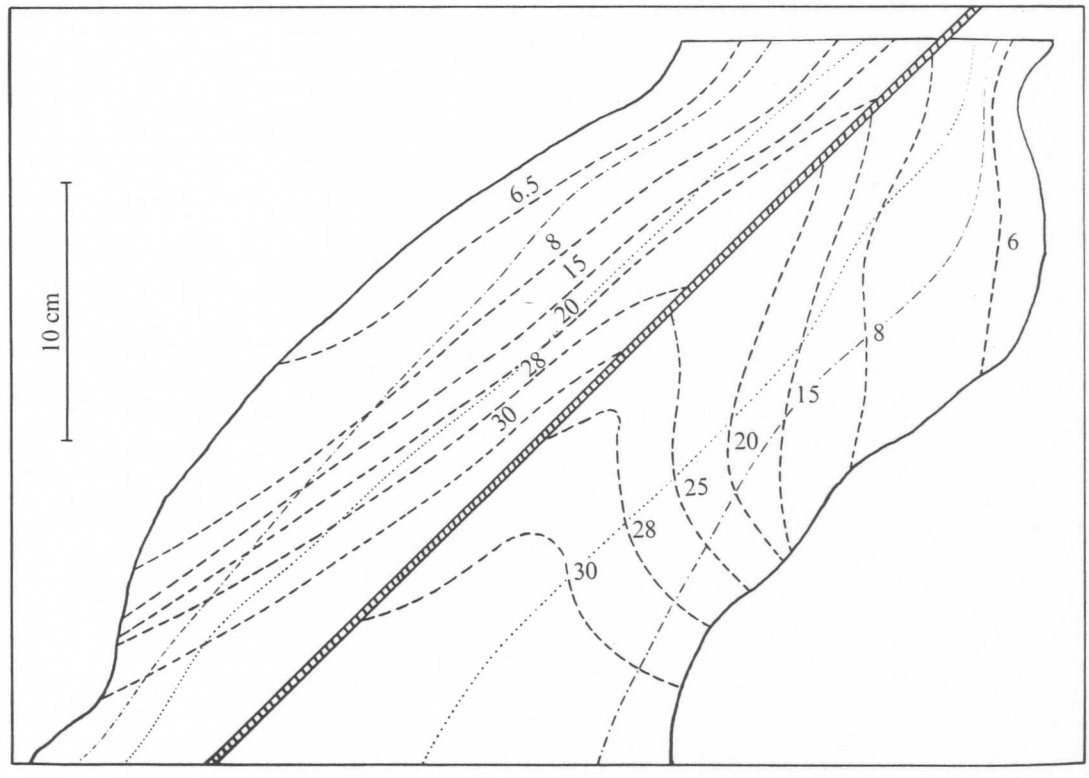

Fig. 26. The distribution of composition, reproduced from Huppert et al. [72], in units of wt% Na_2CO_3, in the solid product obtained by cooling an initially stratified aqueous solution of Na_2CO_3 at a 45° slope. The initial composition increased linearly from 6 wt% at the top of the tank to 13 wt% at the bottom. The solidification front after 55 h is indicated by (· · ·) and after 73 h by (–·–·–).

8. Conclusions

Much further work remains to be done in this exciting field with its many applications. This chapter has developed a series of models which act as a firm foundation for the investigation of many macroscopic solidification effects. Future research will undoubtedly concentrate on the effects of convection within the mushy layer and the change in the rate of solidification that results. Preliminary analyses along this line have already been undertaken by Worster [3, 48]. Additional attention will also be given to the effects of different container geometries, initial stratification in the melt and the presence of three (or more) components about which very little is known – not even the form of the phase diagram in most cases.

Acknowledgements

Parts of this chapter were written during my residence at the University of New South Wales as a Fractional Professor. I am grateful to many members of that University for the kindness they have shown me on my visits. An earlier draft was improved by penetrating comments from M.G. Worster. My general understanding of the solidification problems presented in the chapter has benefited from many stimulating discussions with my colleagues S.H. Davis, D.T.J. Hurle, R.C. Kerr, J.S. Turner, A.W. Woods and M.G. Worster. Mark Hallworth has imaginatively aided me in all my own experiments reported here and produced most of the figures. My recent research, which is partially reported in the chapter, has been generously supported for almost a decade by grants from the British Petroleum Venture Research Unit.

References

[1] H.E. Huppert, J. Fluid Mech. 212 (1990) 209.
[2] J. Stefan, Akad. Math. Natur 98 (S.-B. Wien, 1889) 473.
[3] M.G. Worster, The dynamics of mushy layers, in: Interactive Dynamics of Convection and Solidification, eds. S.H. Davis, H.E. Huppert, U. Müller and M.G. Worster (Elsevier, Amsterdam, 1993) pp. 113–138.
[4] H.S. Carslaw and J.C. Jaeger, Conduction of Heat in Solids (Cambridge University Press, Cambridge, 1959).
[5] M. Abramovitz and I.A. Stegun, Handbook of Mathematical Functions (Dover, New York, 1970).
[6] G. Lamé and B.P. Clapeyron, Ann. Chem. Phys. 47 (1831) 250.
[7] J.M. Hill, One-dimensional Stefan Problems: An Introduction (Longman, London, 1987).
[8] J. Crank, Free- and Moving-Boundary Problems (Clarendon Press, Oxford, 1984).
[9] H.E. Huppert, J. Fluid Mech. 198 (1989) 293.
[10] J.S. Langer, Rev. Mod. Phys. 52 (1980) 1.
[11] P.G. Saffman and G.I. Taylor, Proc. Roy. Soc. London A 245 (1985) 312.
[12] T. Witten and C.M. Sander, Phys. Rev. Lett. 47 (1981) 1400.
[13] Y. Couder, Growth patterns: from stable curved fronts to fractal structures, in: Chaos, Order and Patterns, ed. P. Cvitanovic (Plenum Press, New York, 1991) p. 203.
[14] S.H. Davis, U. Müller and C. Dietsche, J. Fluid Mech. 144 (1984) 133.

[15] C. Dietsche and U. Müller, J. Fluid Mech. 161 (1985) 249.
[16] S.R. Coriell, G.B. McFadden and R.F. Sekerka, Ann. Rev. Mater. Sci. 15 (1985) 119.
[17] J.S. Turner, H.E. Huppert and R.S.J. Sparks, J. Petrol. 17 (1986) 297.
[18] H.E. Huppert and M.G. Worster, Vigorous motions in magma chambers and lava lakes, in: Chaotic Processes in the Geological Sciences, ed. D.A. Yuen, Institute of Mathematics and its Applications Series, Vol. 41 (1991) p. 141.
[19] J.S. Turner, Buoyancy Effects in Fluids (Cambridge University Press, Cambridge, 1979).
[20] K.G. Cox, N.B. Price and B. Harte, The Practical Study of Crystals, Minerals and Rocks (McGraw-Hill, New York, 1974).
[21] K.G. Cox, The interpretation of magmatic evolution, in: Understanding the Earth: A New Synthesis, eds. G.C. Brown, C.J. Hawkesworth and R.C.L. Wilson (Cambridge University Press, Cambridge, 1992).
[22] H.E. Huppert and M.G. Worster, Nature 314 (1985) 703.
[23] L. Rubenstein, The Stefan Problem, AMS Transl. 27 (American Mathematical Society, Providence, RI, 1971).
[24] M.G. Worster, Convective flow problems in geological fluid mechanics, Ph.D. Thesis (University of Cambridge, 1983).
[25] J.W. Rutter and B. Chalmers, Can. J. Phys. 31 (1953) 15.
[26] W.W. Mullins and R.F. Sekerka, J. Appl. Phys. 35 (1964) 444.
[27] S.R. Coriell, M.R. Cordes, W.J. Boettinger and R.F. Sekerka, J. Cryst. Growth 49 (1980) 14.
[28] D.T.J. Hurle, E. Jakeman and A.A. Wheeler, J. Cryst. Growth 48 (1982) 163.
[29] M.E. Glicksman, S.R. Coriell and G.B. McFadden, Ann. Rev. Fluid Mech. 18 (1986) 307.
[30] S.H. Davis, J. Fluid Mech. 212 (1990) 241.
[31] S.H. Davis, H.E. Huppert, U. Müller and M.G. Worster, eds., Interactive Dynamics of Convection and Solidification (Elsevier, Amsterdam, 1993).
[32] G.K. Batchelor, Ann. Rev. Fluid Mech. 6 (1974) 227.
[33] M.G. Worster, J. Fluid Mech. 167 (1986) 481.
[34] T.G.L. Shirtcliffe, H.E. Huppert and M.G. Worster, J. Cryst. Growth 113 (1991) 566.
[35] A.O.P. Chiarelli and M.G. Worster, J. Cryst. Growth (1992).
[36] R.N. Hills, D.E. Loper and P.H. Roberts, Q. J. Appl. Math. 36 (1983) 505.
[37] D.E. Loper, Non-equilibrium effects in a slurry, in: Interactive Dynamics of Convection and Solidification, eds. S.H. Davis, H.E. Huppert, U. Müller and M.G. Worster (Elsevier, Amsterdam, 1993) p. 151.
[38] D.E. Loper, Cont. Mech. Thermodyn. (1992).
[39] W.D. Bennon and F.P. Incropera, Int. J. Heat Mass Transfer 30 (1987) 2161.
[40] R.C. Kerr, A.W. Woods, M.G. Worster and H.E. Huppert, J. Fluid Mech. 216 (1990) 323.
[41] M.G. Worster, H.E. Huppert and R.S.J. Sparks, Earth Planet. Sci. Lett. 101 (1990) 78.
[42] W. Kurz and D.J. Fisher, Fundamentals of Solidification (Trans Tech Publications, Aedermannsdorf, Switzerland, 1986).
[43] S. Flood and J.D. Hunt, Appl. Sci. Res. 44 (1987) 27.
[44] R.C. Kerr, A.W. Woods, M.G. Worster and H.E. Huppert, J. Fluid Mech. 217 (1990) 331.
[45] G. Brandeis and C. Jaupart, Earth Planet. Sci. Lett. 77 (1986) 345.
[46] R.C. Kerr, A.W. Woods, M.G. Worster and H.E. Huppert, Nature 340 (1989) 357.
[47] R.C. Kerr, A.W. Woods, M.G. Worster and H.E. Huppert, J. Fluid Mech. 218 (1990) 337.
[48] M.G. Worster, J. Fluid Mech. 237 (1992) 649.
[49] A.W. Woods and H.E. Huppert, J. Fluid Mech. 199 (1989) 29.
[50] H.E. Huppert and R.S.J. Sparks, J. Fluid Mech. 188 (1988) 107.
[51] S. Ostrach, Laminar flows with body forces, in: Theory of Laminar Flows, ed. F.K. Moore (Princeton University Press, Princeton, 1964).
[52] A.J. Chapman, Heat Transfer (Macmillan, New York, 1984).
[53] R.H. Nilson and M.R. Baer, Int. J. Heat Mass Transfer 25 (1982) 385.
[54] F.J. Spera, D.A. Yuen and D.V. Kemp, Nature 310 (1984) 764.
[55] R.H. Nilson, J. Fluid Mech. 160 (1985) 181.
[56] R.H. Nilson, A.R. McBirney and B.H. Baker, J. Volcanol. Geotherm. Res. 24 (1985) 25.

[57] R.P. Lowell, J. Volcanol. Geotherm. Res. 26 (1985) 1.
[58] A.R. McBirney, J. Volcanol. Geotherm. Res. 7 (1980) 357.
[59] J.S. Turner, Nature 255 (1980) 213.
[60] J.S. Turner and L.B. Gustafson, J. Volcanol. Geotherm. Res. 11 (1981) 92.
[61] A.R. McBirney, B.H. Baker and R.H. Nilson, J. Volcanol. Geotherm. Res. 24 (1985) 1.
[62] A.M. Leitch, Laboratory models of magma chambers, Ph.D. Thesis (Australian National University, 1985).
[63] A.M. Leitch, Various aqueous solutions crystallizing from the side, in: Structure and Dynamics of Partially Solidified Systems, ed. D.E. Loper (Martinus Nijhoff, The Hague, 1987) p. 37.
[64] M.E. Thompson and J. Szekely, Double-diffusive convection during solidification at a vertical wall, in: Structure and Dynamics of Partially Solidified Systems, ed. D.E. Loper (Martinus Nijhoff, The Hague, 1987) p. 59.
[65] M.E. Thompson and J. Szekely, J. Fluid Mech. 187 (1988) 409.
[66] G. Amberg, J. Fluid Mech. (1992) submitted.
[67] H.E. Huppert and J.S. Turner, J. Fluid Mech. 100 (1980) 367.
[68] H.E. Huppert, R.C. Kerr and M.A. Hallworth, Int. J. Heat Mass Transfer 27 (1984) 1395.
[69] H.E. Huppert and J.S. Turner, J. Fluid Mech. 106 (1981) 299.
[70] J.S. Turner, Ann. Rev. Fluid Mech. 17 (1985) 11.
[71] R. Jarvis, Crystallization and melting in geological fluid mechanics, Ph.D. Thesis (Cambridge University, 1991).
[72] D.J. Hebditch, Contribution concerning the solidification problem, in: Moving Boundary Problems in Heat Flow and Diffusion, eds. J.R. Ockendon and W.R. Hodgkins (Clarendon Press, Oxford, 1975).
[73] H.E. Huppert, R.S.J. Sparks, J.R. Wilson and M.A. Hallworth, Earth Planet. Sci. Lett. 79 (1986) 319.
[74] H.E. Huppert, R.S.J. Sparks, J.R. Wilson, M.A. Hallworth and A.M. Leitch, Laboratory experiments with aqueous solutions modelling magma chamber processes – II: Cooling and crystallization along inclined planes, in: Origins of Igneous Layering, NATO Advanced Studies Institute (Reidel, Dordrecht, 1987) p. 539.
[75] W.D. Baines and J.S. Turner, J. Fluid Mech. 37 (1969) 51.
[76] M.G. Worster and A.M. Leitch, J. Fluid Mech. 156 (1985) 301.
[77] W.D. Baines, J.S. Turner and I.H. Campbell, J. Fluid Mech. 212 (1990) 557.